Phytomedicine 150 (2026) 157649

Contents lists available at ScienceDirect

Phytomedicine

journal homepage: www.elsevier.com/locate/phymed

Original Article

Ginsenoside F3 alleviates T cell exhaustion *via* RIPOR2-mediated immunometabolic reprogramming to potentiate anti-PD-1 therapy

Menglin Jiang [a,1], Weiqian Bao [a,1], Lewei He [a,1], Yichun Liang [a], Nanjie Zhou [c], Cuifen Zhang [a], Yuanyuan Song [a], Gangyuan Ma [b], Liqing Chen [b], Kaoling Wen [a], Yicheng Zhao [a], Liang Liu [a,*], Hudan Pan [a,*], Runze Li [a,*]

[a] *Chinese Medicine Guangdong Laboratory /State Key Laboratory of Traditional Chinese Medicine Syndrome, The Second Clinical College of Guangzhou University of Chinese Medicine (Guangdong Provincial Hospital of Chinese Medicine), Guangzhou, Guangdong, China*
[b] *Guangzhou National Laboratory, Guangzhou, 511495, China*
[c] *State Key Laboratory of Oncology in South China, Guangdong Provincial Clinical Research Center for Cancer, Sun Yat-sen University Cancer Center, Guangzhou 510060, China*

A R T I C L E I N F O

Keywords:
T cell exhaustion
RIPOR2
Ginsenoside F3
Non-small cell lung cancer
PD-1 inhibitor

A B S T R A C T

Background: T cell exhaustion (Tex) induced by chronic antigen exposure critically limits cancer immunotherapy. Mechanistic understanding remains incomplete, largely due to inefficient, costly *in vivo* models and a lack of effective interventions. Improved *in vitro* models are therefore urgently needed for mechanism discovery and drug screening.

Methods: An optimized *in vitro* T cell exhaustion model was established *via* chronic anti-CD3 antibody stimulation, achieving robust reproducibility, high cell yields (~10^8), and suitability for high-throughput analyses. Exhaustion was validated functionally and by proteomic profiling across multiple timepoints. Rho family-interacting cell polarization regulator 2 (RIPOR2) was identified as a key regulator and functionally verified through siRNA knockdown assays. Molecular docking screened Ginsenoside F3 (GF3) targeting RIPOR2, and GF3 was tested both *in vitro* and in a mouse NSCLC model with anti-PD-1 therapy.

Results: Our model accurately recapitulated clinical exhaustion phenotypes, notably reproducing diminished cytotoxicity (~60% reduction compared to controls). Proteomics dynamically revealed significant protein alterations during exhaustion, including a ~14-fold downregulation of RIPOR2 mRNA in exhausted T cells. RIPOR2 depletion further exacerbated exhaustion (*e.g.*,Interferon-gamma (IFN-γ) secretion reduced ~30%, Programmed cell death protein 1 (PD-1) increased ~20%). GF3 robustly bound RIPOR2, significantly reversed exhaustion phenotypes (reducing PD-1^+TIM-3^+(Hepatitis A virus cellular receptor 2) cells by ~40%), and restored cytokine production. *In vivo*, GF3 enhanced $CD8^+$ *T* cell infiltration, synergized with anti-PD-1 therapy, and significantly reduced tumor burden (~40% decrease).

Conclusion: RIPOR2 is identified as a critical immunometabolic regulator of T cell exhaustion. GF3-mediated RIPOR2 restoration effectively reverses exhaustion, presenting a novel immunotherapeutic strategy. Our optimized *in vitro* model provides an efficient platform for future mechanistic and pharmacological research.

Abbreviations: BFA, Brefeldin A; cDNA, complementary DNA; CERS4, ceramide synthase 4; CTL, Cytotoxic T lymphocyte; GF3, Ginsenoside F3; HE, Hematoxylin - eosin; ICIs, Immune checkpoint inhibitors; IFN-γ, Interferon-gamma; IL-2, Interleukin-2; IRs, inhibitory receptors; LCMV, Lymphocytic choriomeningitis virus; LLC, Lewis lung carcinoma; MFI, Median fluorescence intensity; NSCLC, Non-small cell lung cancer; PD-1, Programmed cell death protein 1; qRT-PCR, quantitative real-time PCR; RIPOR2, Rho family-interacting cell polarization regulator 2; SPR, surface plasmon resonance Tex,T cell exhaustion; Tpex, T progenitor exhausted cells; TIM-3, Hepatitis A virus cellular receptor 2.

* Corresponding authors.
E-mail addresses: lliu@gzucm.edu.cn (L. Liu), hdpan@gzucm.edu.cn (H. Pan), lirunze@gzucm.edu.cn (R. Li).
[1] These authors contribute equally.

https://doi.org/10.1016/j.phymed.2025.157649
Received 20 August 2025; Received in revised form 31 October 2025; Accepted 30 November 2025
Available online 3 December 2025

Introduction

Cancer immunotherapies such as immune checkpoint inhibitors (ICIs) have achieved remarkable clinical successes, but only 20–40 % of patients respond, leaving the majority with no benefit (Sharma et al., 2017). Therefore, new immunotherapy strategies urgently need to be proposed. T cell exhaustion – a dysfunctional state of T cells characterized by sustained inhibitory receptor expression and loss of effector function – is widely recognized as a major cause of immunotherapy non-response, unable to respond to ICIs treatment(Chow et al., 2022). In exhausted T cells, the ability to secrete cytokines are lost in a stepwise manner: production of Interleukin-2 (*IL-2*) is lost first, followed by Tumor necrosis factor-alpha (*TNF-α),* and eventually Interferon-gamma (*IFN-γ*) (Jenkins et al., 2023). These hypofunctional T cells fail to eliminate tumors, leading to immune evasion and poor clinical outcomes (Jiang et al., 2015). Recent studies have demonstrated that modulating T cell exhaustion can significantly enhance tumor immunotherapy efficacy. Zhou W. et al. found that NAC could inhibit the differentiation of T cells into terminally exhausted cells and improve the therapeutic effect of PD-1 blockade in colorectal cancer (Zhou et al., 2024). Kang TG. et al. discovered that regulating ASXL1 could alleviate T cell exhaustion progression, maintain stem-like T cell properties, and enhance tumor immunotherapy efficacy (Kang et al., 2024). Cheng J. et al. revealed that ETV7 could induce T cell exhaustion progression and promote tumor development (Cheng et al., 2025). Eric Fagerberg. et al. demonstrated that KLF2 plays a crucial role in maintaining T cell effector function and suppressing T cell exhaustion, providing a novel therapeutic target for tumor immunotherapy (Fagerberg et al., 2025). Alleviating T cell exhaustion to restore T cell effector function has therefore become a central challenge in improving immunotherapy efficacy. However, the precise molecular mechanisms driving T cell exhaustion remain incompletely understood, creating bottlenecks in the development of effective therapeutic strategies.

A major obstacle in mechanistic studies has been the lack of robust experimental models that faithfully recapitulate T cell exhaustion. Traditional *in vivo* models, such as chronic lymphocytic choriomeningitis virus (*LCMV*) infection, established the concept of exhaustion but are labor-intensive and yield limited cell numbers (Belk et al., 2022; Moskophidis et al., 1993). Recently, researchers have developed *in vitro* T cell exhaustion assays by chronically stimulating T cells *ex vivo*. For example, Belk et al. (2022) reported a chronic anti-CD3/anti-CD28 stimulation model that produces large numbers ($\sim 10^8$) of exhausted $CD8^+$ *T* cells from a single mouse within days. This *in vitro* model recapitulates the phenotypic and epigenetic hallmarks of terminally exhausted T cells observed in tumors and chronic infection (Belk et al., 2022). Indeed, continuous TCR activation in culture can mimic the tumor milieu, inducing high co-inhibitory receptors (*e.g.* PD-1, TIM-3) and global chromatin changes analogous to those in tumor-infiltrating lymphocytes. Such models have enabled high-throughput approaches (*e.g.* CRISPR screens) to identify genetic regulators of exhaustion. Recent studies have begun to map the transcriptional and epigenetic programs of exhausted T cells (Chow et al., 2022; J. E. J. E. Wu et al., 2023), but translating these findings into *bona fide* "T cell rejuvenation" therapies is still an urgent, unmet need.

Emerging evidence points to immunometabolic dysregulation as a key driver of T cell exhaustion and a promising avenue for intervention (Ma et al., 2025; Mortazavi Farsani et al., 2025). In the tumor microenvironment (TME), chronic antigen stimulation is compounded by a harsh metabolic context – limited glucose and oxygen, and accumulation of lactic acid – which fosters T cell dysfunction (Peralta et al., 2024) Exhausted T cells undergo profound metabolic remodeling, including impaired glycolysis and mitochondria, that reinforces their hypofunctional state (Peralta et al., 2024). Consistently, our proteomic analysis (detailed below) indicates that metabolic pathways are prominently altered during chronic stimulation. Targeting metabolic pathways has therefore become a major focus in developing *sensitizer* drugs to enhance immunotherapy response (Agarwala et al., 2024). The consensus is that *overcoming metabolic dysfunction* in T cells can bolster their effector functions and potentially prevent exhaustion, representing a cutting-edge direction for immunotherapy drug development (Chow et al., 2022).

Another crucial consideration in next-generation immunotherapy is the trend toward multi-target synergy and holistic treatment of tumors. Small-molecule drugs are especially attractive in this regard because of their ability to penetrate tissues and concurrently modulate various intracellular signaling and metabolic pathways. More generally, combining metabolic or immunomodulatory small molecules with ICIs is emerging as a promising strategy to overcome resistance (Singh et al., 2023). Preclinical studies demonstrate that small-molecule metabolic modifiers can increase TIL infiltration and function, yielding synergistic anti-tumor effects when used alongside checkpoint inhibitors or CAR T cells (Agarwala et al., 2024). Furthermore, certain natural compound derivatives have shown potential in multi-target immunotherapy settings. Our team's previous research found that ginseng polysaccharides - the main active components of Panax ginseng C.A.Mey. - significantly enhanced PD-1 monoclonal antibody efficacy in NSCLC models ($n = 6$) by modulating gut microbiota and the kynurenine/tryptophan ratio, demonstrating 75.2 % tumor growth inhibition in combination therapy compared to PD-1 monotherapy, along with marked improvements in tumor volume, weight and survival outcomes (Huang et al., 2022). It is suggested that ginseng has the effect of enhancing tumor immunotherapy, but the relationship between it and T-cell exhaustion has not yet been clarified. Ginsenosides, bioactive components of Panax ginseng C.A.Mey., have immunomodulatory properties and can influence both immune and metabolic pathways (Wang et al., 2024) Combining ginsenosides with checkpoint blockade has yielded encouraging results in preclinical models – for example, ginsenoside Rh2 or Compound K enhanced anti-PD-(l)1 therapy by increasing intratumoral $CD8^+$ *T* cell infiltration and function (Huang et al., 2023; Shang et al., 2025). These trends underscore that rational combination therapies leveraging small molecules to target multiple facets of the tumor and immune system are a key frontier in improving response rates. In this context, there is considerable interest in discovering new small molecules that can simultaneously reinvigorate exhausted T cells and modulate the tumor microenvironment, thereby synergizing with existing immunotherapies.

In this study, we investigate the mechanisms of $CD8^+$ *T* cell exhaustion and propose a novel intervention strategy using a natural small molecule. We establish an *in vitro* chronic stimulation model of T cell exhaustion to generate sufficient exhausted T cells for multi-omics analysis. Then, using high-throughput proteomics, we identify key regulatory proteins that are dysregulated early in the exhaustion process, with a particular focus on metabolic regulators. We validate the role of RIPOR2 in maintaining T cell function both in murine models and in patient tumor-infiltrating T cells. Finally, through a combination of molecular docking and functional assays, we identify Ginsenoside F3 (GF3) – a rare ginsenoside – as a small-molecule compound that targets RIPOR2. We demonstrate that GF3 can alleviate T cell exhaustion, and synergize with PD-1 blockade to improve anti-tumor immunity in a non-small cell lung cancer (NSCLC) model. Our findings reveal a new mechanism whereby it reinforces T cell metabolic/functional fitness *via* RIPOR2, thereby alleviating exhaustion. This multi-target approach – intervening in both T cell intrinsic regulators and the tumor immune environment – represents a promising strategy to overcome the low response rates and lack of effective sensitizers in current immunotherapy.

Materials and methods

Mice

C57BL/6 J mice (male, 6–8 weeks old, 20–30 g; Guangzhou Vital River Laboratory Animal Technology Co., Ltd.). Approval for all

experimental procedures in this study was granted by the Animal Ethics Committee of the Guangdong Provincial Hospital of Traditional Chinese Medicine (Registration number:2022,034;Date:December 10, 2023; License number: SYXK (Yue) 2018–0092). The mice were housed in the barrier facility of the Guangdong Provincial Academy of Chinese Medical Sciences under controlled environmental conditions: ambient temperature maintained at 22–24 °C, relative humidity at 40–50 %, with *ad libitum* access to food and water. A 12-h light/dark cycle was implemented to ensure the animals were kept in optimal comfort throughout the study period.

Cell culture

The lewis lung carcinoma cells (LLC cells), H1299, A549 and Jurkat cell lines were obtained from the Cell Bank of Chinese Academy of Sciences (CAS, Shanghai, China). LLC cells were cultivated in DMEM medium. Other cells were cultivated in RPMI 1640 medium. The culture media were also enriched with 10 % fetal bovine serum (FBS), 100 U Pen/Strep and maintained at 37 °C in an environment with 5 % CO_2. Main reagents and materials are shown in Table S1.

In vitro T cell exhaustion assay

After euthanasia *via* isoflurane inhalation, spleens were aseptically harvested and mashed through a 70 μm cell strainer to obtain single cell suspensions. Cells were counted and then resuspended in Robosep buffer (PBS + 2 % FBS + 1 mM EDTA) to a concentration of 1×10^8 cells/ml. $CD8^+T$ cells were isolated *via* a negative selection kit (STEMCELL Technologies, 19,853) according to the manufacturer's protocol and then resuspended in RPMI 1640 with 10 % FBS, 100 U Pen/Strep, 50 nM of B-mercaptoethanol and supplemented with 10 ng/ml of mouse IL-2. Cells were seeded at a concentration of 1 million cells/ml on plates coated with 5 μg/ml of anti-CD3 and 2 μg/ml of anti-CD28. Cells were kept on these activation plates for 48 h at the beginning of all experiments. $CD8^+$ *T* cell purity was verified *via* flow cytometry and the status of mycoplasma infection in cells was also detected. Cells were passaged every two days and maintained at a seeding concentration of 1 million cells/ml.

Following 48 h activation, chronically stimulated cells were passaged every two days at 1×10^6 cells/ml onto fresh anti-CD3-coated plates (5 μg/ml), while acute cells were maintained at the same density in uncoated plates during each passage(in the continued presence of 10 ng/ml IL-2). Cells were analyzed on Day 0, 2, 4, 6, 8, 10 as described in the Results.

Measurement of inhibitory receptors (IRs)

$CD8^+$ T cells stimulated until Day 4, 6, 8, 10 were collected for detection of surface inhibitory receptor markers(IRs). Cells were washed once with cell staining buffer, stained with Ghost Dye Violet 540, and incubated at 4 °C for 30 min, followed by surface antibody staining. They were then washed once times with cell staining buffer again. Finally resuspension in cell staining buffer before flow cytometry analysis. Flow cytometry was performed using a CytoFlex S (Beckman), FlowJo v.10.8 was used for data analysis. All experiments were performed with at least three biological replicates. Antibodies used (at 1:200 unless otherwise noted) were PD1-PE, TIM3-BV421 .

Measurement of cytokine production

Cytokine secretion was assessed after restimulation with anti-CD3 (3 μg/ml). Cells were stimulated with anti-CD3 for 90 min, followed by brefeldin A (BFA, 10 μg/ml) treatment for 3–4 h to inhibit protein transport. Intracellular cytokines were then analyzed by flow cytometry. Cells were simultaneously labeled with Ghost Dye Violet 540 for 30 min at 4 °C, washed twice, and fixed for 20 min using a Cyto-Fast Fix/Perm Buffer Set (BioLegend) at room temperature. After washing, cells were stained for intracellular cytokines for 1 h at room temperature, followed by two additional washes and resuspension in cell staining buffer. Subsequently, Cell samples were analyzed by flow cytometry (Beckman), with subsequent data processing performed using FlowJo software as described previously. Antibodies used were TNF-α-PE, IFN-γ-BV421.

Protein sample preparation for proteomics

At each time point (Day 0/2/4/6/8/10), 3×10^6 cells from both acute and chronic stimulated cells were pelleted by centrifugation (500 g, 5 min), washed 2–3 times with ice-cold PBS, and carefully aspirated to remove residual supernatant. Cell pellets were flash-frozen in liquid nitrogen (1 min exposure) and stored at −80 °C. After complete sample collection, all specimens were transported on dry ice to Bioprofile Biotechnology Co., Ltd (Shanghai) for standardized proteomic sample preparation and mass spectrometry analysis.The detailed protein pretreatment procedure is illustrated in Fig. S2A.

scRNA-seq data analysis

Raw sequencing data from the GSE99254 single-cell RNA-seq dataset were standardized as follows: alignment, quality control, and gene expression matrix construction were performed using Cell Ranger (v6.1.2), with low-quality cells (expressing <200 genes or >15 % mitochondrial genes) excluded. Subsequent data integration and batch effect correction were conducted using Seurat (v4.3.0) with the Harmony algorithm. After PCA dimensionality reduction (top 30 principal components) and UMAP visualization, cells were clustered using the Louvain algorithm with hierarchical refinement. Downstream analyses focused exclusively on T cells, which were annotated based on canonical markers (Guo et al., 2018): $CD8^+$ *T* cells were subclassified into effector cells (CD8-C3-CX3CR1, characterized by high expression of GZMB, PRF1, and CX3CR1) and exhausted cells (CD8-C6-LAYN, marked by elevated PDCD1, HAVCR2, LAYN, and TOX). Expression matrices of these two $CD8^+$ *T* cell subsets were extracted, and RIPOR2 expression differences between effector and exhausted tumor-infiltrating T cells from clinical lung cancer patients were compared using the "FindMarkers" function (Wilcoxon rank-sum test), with the distribution of RIPOR2 expression visualized *via* violin plots.

Mouse T cell RIPOR2 knockdown assay

Following 48 h activation with anti-CD3/CD28 (BioXcell,1:1000), primary mouse $CD8^+$ *T* cells were subjected to RIPOR2 knockdown using the ProteanFect Max Primary Mouse Immune Cell Transfection Kit according to the manufacturer's protocol. Transfection efficiency was assessed by flow cytometry on the day after transfection, as shown in the results figure. Subsequently, cells were maintained under chronic stimulation to induce T cell exhaustion, and flow cytometry was used to compare exhaustion differentiation and effector function between RIPOR2-knockdown (KO) and control (NC) T cells.

Transcription factor detection

Samples were washed twice with PBS, then stained with Ghost Dye Violet 540 and surface markers as previously described. Cells were fixed overnight using a nuclear permeabilization/fixation kit(BD, Cat#562,574) washed twice with wash buffer the following day, and stained for nuclear transcription factor Tcf-1 for 1 h. After two additional washes, cells were resuspended in 200 μl PBS and acquired by flow cytometry, with data analyzed using FlowJo software. Antibodies used included: TCF-1-RB705.

In vitro killing assay

LLC cells were plated in 96-well plates (10,000 cells/well in 100 μl medium) and allowed to adhere for 16 h before adding chronically or acutely stimulated T cells at varying effector-to-target ratios (1.25:1 to 10:1) along with 5 μg/ml anti-CD3 and anti-CD28 for restimulation. After 24 h co-culture, supernatants were collected and wells were washed once with PBS. Tumor cells were then detached using 100 μl EDTA-free trypsin (5 min, RT), with digestion terminated by adding 200 μl complete medium. For Cytotoxic T lymphocyte (CTL)-mediated tumor cell killing assay, cells were washed twice with PBS (800 × *g*, 5 min, RT), surface-stained with anti-CD8 antibody (20 min, RT), washed with Annexin Binding Buffer, then stained with 0.5 μl FITC Annexin V (15 min, RT) followed by resuspension in 400 μl Annexin Binding Buffer. Subsequently, 5 μl Propidium Iodide (PI) was added (5 min, RT). All samples were kept on ice in the dark until flow cytometry analysis to quantify tumor cell killing ($CD8^-$Annexin V^+PI^+ populations).

Mouse NSCLC models and therapeutic intervention

All the mice were fed adaptively for 1 week under specific pathogen-free conditions with food and water provided *ad libitum*. Then Mice were intravenously injected *via* the tail vein with 4×10^5 LLC cells/100 μl to establish the NSCLC model. Next day, the mice were randomly assigned to the control group, model group, and intervention groups (ginsenoside F3, PD-1 blockers, and combination groups). Ginsenoside F3 (GF3,Purity ≥ 99.95 %; PubChem CID: 46,887,678; CAS: 62,025–50–7), whose structure is illustrated in Fig. S5A and purchased from TargetMol (Shanghai, China),was suspended in 0.5 % carboxymethylcellulose sodium (CMC—Na) and administered at a dose of 5 mg/kg (i.p., daily). The PD-1 blockers (clone RMP1–14; Selleck) was diluted in PBS to 200 μg per mouse (i.p., every three time days). The mice in both model and control groups were administered the same volume of saline (i.p., daily). The body weight were measured every three days. After 29 days, the weights of the lung tumors were measured.

Hematoxylin-eosin (HE) staining

The left lung lobe of mice was excised, cut into small pieces (approximately 2–3 mm^3), and fixed with 4 % paraformaldehyde. After dehydration with gradient ethanol, the tissues were paraffin-embedded and cut into 4-micron-thick sections using a microtome. The sections were then dewaxed with xylene, rehydrated with gradient ethanol, and stained with hematoxylin for 5–10 min. After rinsing with running water, the sections were immersed in 1 % hydrochloric acid alcohol differentiation solution for 5–10 s, followed by bluing with 0.1 % ammonia water for 30 s to visualize nuclei as clear blue-purple. After counterstaining with eosin for 1–2 min, the sections were routinely dehydrated, cleared, and mounted with neutral balsam, then observed and photographed under a light microscope, followed by subsequent analysis using ImageScope x64 software.

Mouse tumor tissues flow cytometry analysis

Tumor tissues were cut into small pieces and placed into gentle MACS 25C Tubes C (Miltenyi), followed by the addition of 1 ml of medium containing collagenase D (1 mg/ml) and DNase I (0.2 mg/ml) as the digestion solution. Using tissue dissociator (Miltenyi), the 37 °C-m-LDK-1 program was selected to obtain cell suspensions. The suspensions were then transferred to 15 ml centrifuge tubes for centrifugation, resuspended in 2 ml of cell staining buffer, filtered through a 70 μm strainer, and centrifuged again. Next, 1 ml of red blood cell lysis buffer (Beyotime,Cat#C3702) was added for lysis on ice for 10 min, followed by centrifugation to obtain single-cell suspensions. Subsequently, Cells were pre-treated with CD16/CD32 blocker (15 min), then stained with viability dye (Ghost Dye Violet 540, 30 min) and surface markers (CD45/CD3/CD4/CD8, 20 min) at 4 °C. Flow cytometry was performed on a CytoFLEX S (Beckman) with FlowJo v10.8 analysis.

Cell proliferation assay

Cell proliferation was examined using the Cell Counting Kit-8 (CCK8). H1299, A549 and LLC cells were seeded in 96-well microplates (2000 cells/well) After cell adhesion, the cells were treated with 100 μl various concentrations (0, 0. 1, 1, 10, 100, μM) of GF3 for 24 h, 48 h or 72 h. Jurkat cells were seeded in 96-well microplates (20,000 cells/well). As Jurkat cells are suspension cells, drug intervention was performed directly on the seeding day using GF3-containing medium at different concentrations for 24 h and 48 h. Then 10 μl of CCK8 solution was added to each well, and the cells were further incubated for 1 h. The microplate reader was used to measure the optical density (OD) at 450 nm. All of the experiments were performed three independent times.

Quantitative real-time PCR

Total RNA was extracted from T cells using TRIzol reagent (TRANS), and complementary DNA (cDNA) was synthesized *via* reverse transcription according to the manufacturer's protocol (TRANS). Quantitative real-time PCR (qRT-PCR) was performed on a ViiA™ 7 Real-Time PCR System using SYBR Green (AG). The relative gene expression levels were calculated using the 2^(-ΔΔCt) method, with β-actin as the internal reference gene. All primers were synthesized by Sangon Biotech (Shanghai, China), and their sequences are provided in Supplementary Table S2.

Statistical analyses

SPSS Statistics 25.0 and GraphPad Prism 9.0 were used for the statistical analysis.Data normality was first assessed using the Shapiro-Wilk test. Normally distributed data are presented as mean ± standard deviation ($\bar{x} \pm$ SEM), while non-normally distributed data ($p < 0.05$) are expressed as median (interquartile range) [P50 (P25-P75)]. For independent samples with normal distribution, homogeneity of variance was examined using Levene's test. Two-group comparisons were performed using Student's *t*-test when variances were equal or Welch's *t*-test when variances were unequal. Multiple group comparisons with normal distribution and equal variances were analyzed by one-way ANOVA, while Brown-Forsythe or Welch ANOVA was used for unequal variances, followed by Tukey's HSD post-hoc test. Non-normally distributed data were analyzed using the Kruskal-Wallis test, with Bonferroni-corrected Mann-Whitney U tests for post-hoc comparisons. **P*-value under 0.05, ***P*-value under 0.01 and ****P*-value under 0.001 were thought to be statistically significant.

Results

Chronic anti-CD3 antibodies stimulation in vitro induces the molecular phenotype of $CD8^+$T cell exhaustion

To obtain sufficient $CD8^+$ *T* cells with bona fide exhausted phenotype for high-throughput analyses and drug screening, we established an *in vitro* T cell exhaustion model using chronic anti-CD3 stimulation (Belk et al., 2022). As shown in Fig. S1, naïve $CD8^+$ *T* cells were isolated from mouse spleens and activated with anti-CD3/CD28 for 2 days to induce initial expansion. Subsequently, the cells were continuously stimulated with plate-bound anti-CD3 antibody for up to 10 days (with regular restimulation every 2 days) to drive them into an exhausted state. This abundance of cells enabled reliable downstream high-throughput proteomic profiling.

We first confirmed that the chronically stimulated $CD8^+$ *T* cells acquired a canonical exhausted phenotype over time. Starting with highly pure (≥95 %) resting $CD8^+$ *T* cells (Fig. S1A, B), robust initial activation

was observed after 2 days of CD3/CD28 stimulation (>90 % cells became $CD25^+$; Fig. S1C). We then tracked the expression of inhibitory receptors *PD-1* and *TIM-3* during chronic stimulation as hallmarks of exhaustion. By day 4 of continuous anti-CD3 exposure, a distinct double-positive $PD\text{-}1^+TIM\text{-}3^+$ subpopulation emerged (≈13.4 % of $CD8^+$ cells), indicating onset of the exhaustion program (Fig. 1A, B). This $PD\text{-}1^+TIM\text{-}3^+$ fraction expanded markedly to ~58.1 % by day 6. Further stimulation to day 8 and 10 did not increase the proportion beyond this peak (day 8: 54.0 %; day 10: 51.6 %), suggesting a plateau where most cells susceptible to exhaustion had already converted by day 6 (Fig. 1B). The persistent high-level expression of multiple inhibitory receptors (such as PD-1 and TIM-3) on these cells is a defining feature of exhausted T cells.

Then, the effector functions of T cells during the course of exhaustion induction were assessed. A hallmark of T cell exhaustion is the progressive loss of cytokine secretion and cytotoxicity (Jenkins et al., 2023). Consistently, we found that chronically stimulated $CD8^+$ *T* cells exhibited severely impaired function by day 6. When stimulated acutely (2 days, *Tac* condition), $CD8^+$ *T* cells produced abundant interferon-γ (IFN-γ), as measured by Flow Cytometry (78.13±2.26 units). In contrast, day-6 chronically stimulated cells (*Tex* condition) showed an ~20-fold reduction in IFN-γ secretion (3.86±1.03). This loss of function was highly significant ($^{**}p < 0.001$) and became even more pronounced by

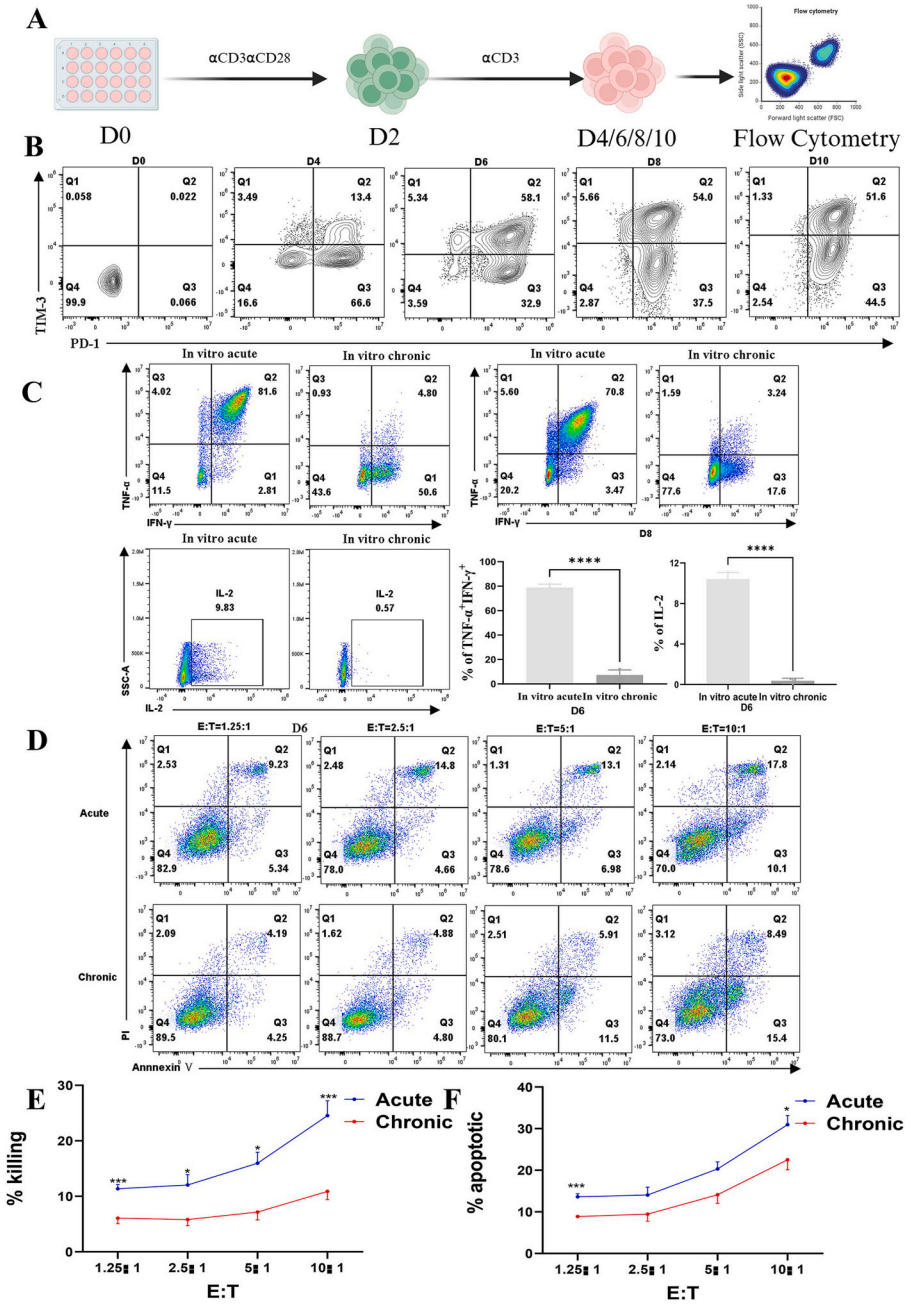

Fig. 1. Establishment of mouse CD8 T cell exhaustion model *in vitro*. A. *In vitro* T cell exhaustion model establishment: Following αCD3/αCD28 activation, chronic αCD3 stimulation was maintained through Day 10 (D10), with T cell exhaustion status evaluated by flow cytometry. B. Expression of surface inhibitory receptors PD-1 and TIM-3 during chronic stimulation. C. Cytokine secretion (TNF-α, IFN-γ, IL-2) by *in vitro* chronic and *in vitro* acute cells at D6, showing representative flow cytometry data and statistical results($n = 3$). Cytokine production (TNF-α, IFN-γ) in both groups at D8. D. Tumor cell (LLC) killing activity by chronic and acute cells at various effector-to-target ratios (E:*T* = 1.25:1, 2.5:1, 5:1, 10:1), showing representative experimental results. E. Statistical results of T cell-mediated tumor cell killing at different effector-to-target (E:T) ratios. Blue represents transiently stimulated cells; red indicates chronically stimulated cells ($n = 3$). F. Statistical results of tumor cell apoptosis at different effector-to-target (E:T) ratios. Blue represents transiently stimulated cells; red indicates chronically stimulated cells ($n = 3$).

day 8 (Fig. 1C). The stepwise cytokine attrition we observed (with IL-2 and TNF-α likely lost before IFN-γ) aligns with the known hierarchy of dysfunction in T cell exhaustion. By day 8, our *Tex* cells represent a profoundly exhausted state with regard to cytokine production.

One of the most important phenomena, the T cells' ability to kill tumor cells using a co-culture assay with LLC (Lewis lung carcinoma) target cells was tested. Across multiple effector-to-target ratios, the chronic stimulation group showed markedly reduced cytotoxicity compared to acutely stimulated effectors (Fig. 1D–F). Fewer tumor cells were killed and correspondingly fewer apoptotic targets were detected when using day-6 exhausted T cells as effectors ($p < 0.05$). Thus, chronic TCR engagement drove $CD8^+$ *T* cells into a state of diminished effector capacity, mirroring the functional exhaustion seen in tumors.

High-Throughput proteomics reveals metabolic regulators and identifies RIPOR2 as a key factor in T cell exhaustion

Leveraging the large numbers of cells from our *in vitro* system, we performed high-throughput proteomic screening to systematically identify proteins associated with $CD8^+$ *T* cell exhaustion. We compared the global protein expression profiles of chronically stimulated cells (*Tex*) *versus* acutely stimulated effector cells (*Tac*) over multiple time points (days 0, 2, 4, 6, 8, 10; experimental design in Fig. S2A). Principal component analysis (PCA) of the proteomic data showed tight clustering of replicate samples, indicating excellent reproducibility and stable experimental conditions. Strikingly, starting at day 4, the *Tex* samples began to segregate clearly from *Tac* along the principal components (Fig. S2B). This divergence by day 4 correlates with our phenotypic observations that exhaustion traits ($PD\text{-}1^+TIM\text{-}3^+$ cells) first become evident around that time. By day 6 and beyond, the separation in PCA space was even more pronounced, reflecting broad molecular differences between exhausted *versus* non-exhausted T cells.

Unsupervised hierarchical clustering of the proteome data further illustrated the dynamics of exhaustion. The protein expression patterns of *Tex* samples at days 4, 6, and 8 were highly similar to each other, forming a tight cluster distinct from the *Tac* counterparts (Fig. 2A). This suggests that once the exhaustion program is established (~day 4), it is maintained through day 8 with a relatively stable signature. Consistent with T cells acquiring exhaustion markers, known inhibitory receptors such as PD-1 (*Pdcd1*) and TIM-3 (*Havcr2*) were significantly upregulated in the *Tex* group compared to *Tac* from day 4 onward (Fig. S2D, E). These proteins are canonical markers of exhausted T cells and their increased expression in our proteomic data validates that the *Tex* cells had indeed assumed an exhaustion phenotype.

Differential protein expression analysis was performed between *Tex* and *Tac* at each time point. The number of differentially expressed proteins (DEPs) was low at day 0–2 (as expected, prior to exhaustion induction) but increased sharply from day 4 onward, peaking at day 6 (Fig. 2B, C). This timeline aligns with our flow cytometry results where exhaustion became appreciable by day 4 and more prominent by day 6. It suggests that day 4 is a turning point when extensive proteomic reprogramming occurs as T cells transition into exhaustion. We were particularly interested in proteins that changed early (day 4) and remained dysregulated thereafter, as such factors might initiate and reinforce the exhaustion program. A Venn analysis of DEPs at days 4, 6, and 8 revealed 1445 proteins that were commonly differentially expressed in exhausted *vs* non-exhausted cells across all three time points (Fig. S2F). These shared DEPs likely represent core, persistent alterations associated with the exhaustion state.

Pathway enrichment analysis of the common DEPs highlighted metabolic pathways as significantly over-represented (Fig. 2C and Fig. S2G). Gene Ontology (GO) and KEGG analysis showed that proteins involved in cellular metabolism – including glycolysis, oxidative phosphorylation, and amino acid metabolism – were prominently enriched among those differentially expressed in exhaustion. This finding accords with the growing appreciation that metabolic dysfunction is intertwined with T cell exhaustion.

Among the early and sustained changes, one protein stood out, RIPOR2 (*Rho family-interacting cell polarization regulator 2*). RIPOR2 (also known as FAM65B) showed a striking pattern – it was significantly *downregulated* in *Tex* cells compared to *Tac* cells at day 4, and its expression continued to decline at days 6 and 8 (Fig. 2C). In fact, RIPOR2 was one of the most consistently suppressed proteins in exhausted T cells relative to activated effector T cells. We validated the proteomic result at the mRNA level by comparing RIPOR2 gene expression in exhausted *vs* non-exhausted T cells. Consistent with the protein data, RIPOR2 transcript levels were dramatically lower in the *Tex* group (chronic stimulation) than in the *Tac* group (acute stimulation). Quantitative PCR on day 6 cells showed RIPOR2 mRNA in *Tex* was only ~1/15 (~7 %) of that in *Tac* (0.095 ± 0.016 vs 1.464 ± 0.125; $^{**}p < 0.001$, Fig. 2D). This ~14-fold reduction corroborates that RIPOR2 is transcriptionally repressed during the development of exhaustion. Together, the proteomic and transcript data establish RIPOR2 as a novel differentially expressed molecule associated with T cell exhaustion.

To examine the clinical and *in vivo* relevance of RIPOR2 in T cell exhaustion, we turned to datasets of tumor-infiltrating lymphocytes (TILs) and patient samples. Analysis of a public single-cell RNA-seq dataset of $CD8^+$ TILs from a murine melanoma model (GSE175408) revealed that RIPOR2 expression is significantly lower in exhausted T cells compared to other T cell subsets *in vivo*. Specifically, in tumor-infiltrating $CD8^+$ *T* cells, the subset identified as terminally exhausted T cells had markedly reduced RIPOR2 levels relative to **resting/naïve cells* and effector T cells (one-way ANOVA, $p < 0.05$ vs naïve; $^{**}p < 0.001$ vs effector; Fig. S3A). Even progenitor exhausted (pre-exhausted) T cells in the tumor showed a trend of RIPOR2 downregulation, which became more pronounced in the terminally exhausted subset (Fig. S3A). This gradation – higher RIPOR2 in functional effector cells, lower in exhausted cells – mirrors our *in vitro* findings and supports an *in vivo* link between RIPOR2 loss and the exhausted phenotype.

We observed a similar pattern in human tumor samples. In a single-cell transcriptomic dataset of T cells from NSCLC patients (GSE99254, from Guo et al.) (Guo et al., 2018), we identified distinct $CD8^+$ *T* cell clusters corresponding to functional effector and exhausted states. Notably, one cluster annotated as *CD8-C3-CX3CR1*$^+$ represented effector $CD8^+$ *T* cells (high in cytotoxic genes, *CX3CR1* being a marker of terminal effectors), while another cluster *CD8-C6-LAYN*$^+$ represented exhausted $CD8^+$ *T* cells (expressing exhaustion markers such as *LAYN, PDCD1, HAVCR2*, etc.). When we compared *RIPOR2* expression between these clusters, we found that RIPOR2 was highly expressed in the effector CD8-C3 population but markedly low in the exhausted CD8-C6 population (Fig. 2E and Fig. S3B, C). This dichotomy in clinical samples reinforces the notion that RIPOR2 downregulation is a feature of exhausted T cells in cancer. Importantly, Guo et al. also reported that a higher ratio of "pre-exhausted" (progenitor) to exhausted T cells in NSCLC was associated with better patient survival. Given that we see higher RIPOR2 in those less-exhausted (effector-like) T cells, one can speculate that $RIPOR2^{high}$ T cells may retain more functionality and confer improved immunity.

To directly test whether RIPOR2 plays a functional role in restraining T cell exhaustion, we performed loss-of-function experiments. Using siRNA-based knockdown, we silenced RIPOR2 in $CD8^+$ *T* cells ex vivo and examined the effects on exhaustion phenotypes. RIPOR2 knockdown was confirmed by >70 % reduction in protein levels (Fig. S4A, B). Strikingly, T cells with RIPOR2 knockdown exhibited *exacerbated exhaustion*: the frequency of $PD\text{-}1^+TIM\text{-}3^+$ cells increased further compared to control T cells under the same chronic stimulation conditions (Fig. 2F). In parallel, the proportion of T cells positive for the transcription factor TCF-1 (encoded by *TCF7*) was reduced upon RIPOR2 silencing (Fig. 2F).

Consistently, RIPOR2-deficient T cells showed further loss of effector function. We stimulated chronically exhausted T cells (day 6 *Tex*) with PMA/ionomycin and measured intracellular cytokines. Control

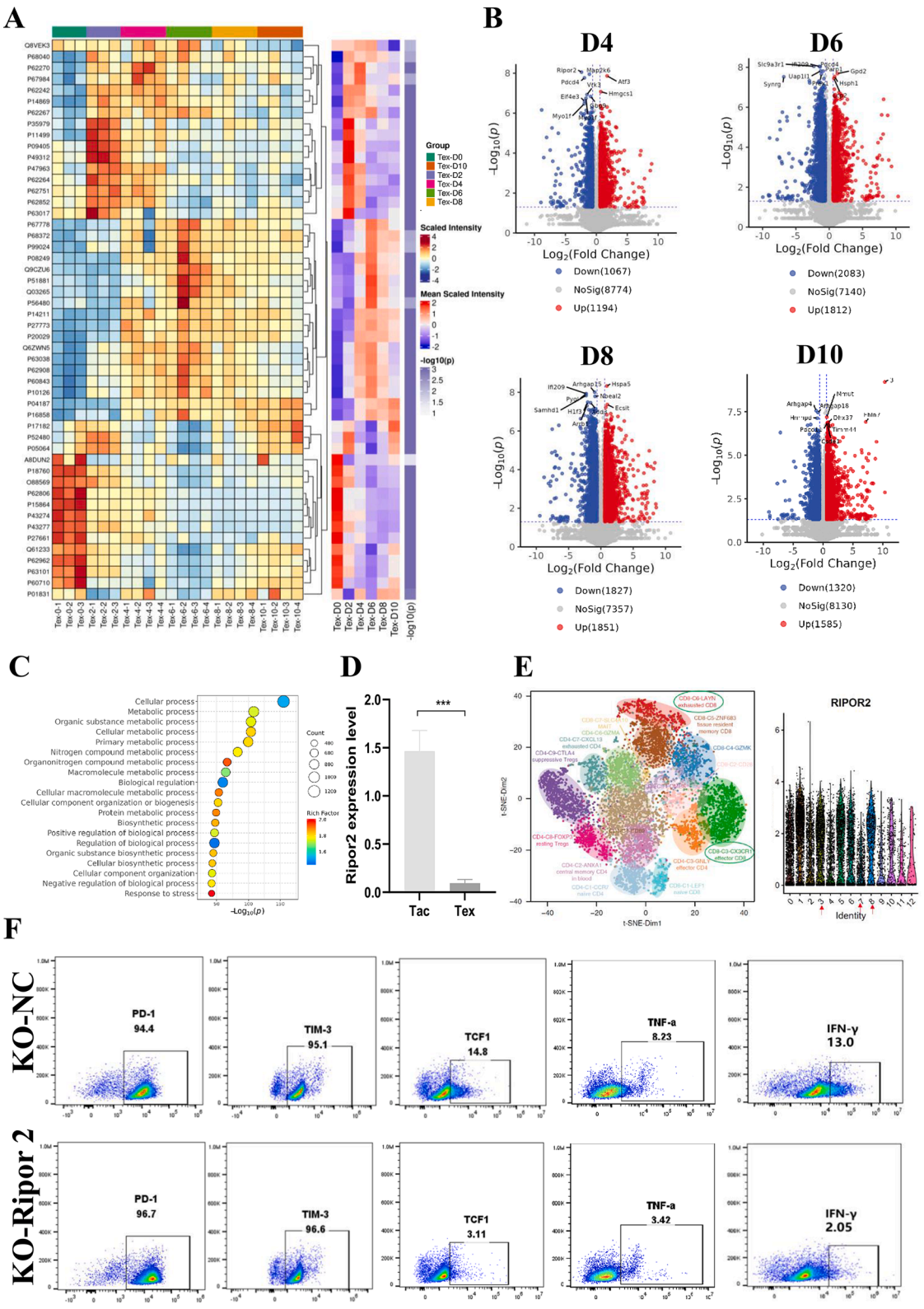

Fig. 2. High-throughput proteomic analysis results and the impact of RIPOR2 in T cell exhaustion progression. A. Heatmap of Tac and Tex proteins at D0/D2/D4/D6/D8/D10. B. Volcano plots of differentially expressed proteins between Tex and Tac at D4, D6, and D8. Blue indicates downregulated proteins, red represents upregulated proteins, and gray denotes non-significant proteins. C. GO analysis in the proteome. D. mRNA expression of RIPOR2 in the *in vitro* exhaustion model, with statistical results ($n = 3$). E. Expression of RIPOR2 in effector and exhausted T cells from the GSE99254 dataset. F. Expression of surface inhibitory receptors (PD-1, TIM-3) and transcription factor TCF-1 in $CD8^+$ *T* cells following RIPOR2 knockdown. NC: normal CD8+ *T* cells; KO: RIPOR2-knockdown $CD8^+$ *T* cells. Shown are representative experimental results. G. Cytokine production (TNF-α and IFN-γ) of $CD8^+$ *T* cells after RIPOR2 knockdown. NC: normal $CD8^+$T cells; KO: RIPOR2-knockdown $CD8^+$ *T* cells. Data show one representative experiment.

exhausted T cells produced low levels of *TNF-α* and *IFN-γ*, as expected (baseline exhaustion blunts cytokine production). Upon RIPOR2 knockdown, cytokine production was even more impaired: the fraction of cells co-producing TNF-α and IFN-γ dropped, and the median fluorescence intensity (MFI) of each cytokine per cell also decreased substantially. For example, in control exhausted T cells the TNF-α^+IFN-γ^+fraction was modest (values in parentheses), but in RIPOR2-knockdown exhausted T cells it was almost halved (3.42 % *vs* 8.23 % for TNF-α^+; 2.05 % *vs* 13.0 % for IFN-γ^+; Fig. 2G).

Finding a small molecule-ginsenoside F3 targets RIPOR2 to alleviate T cell exhaustion

Given the pivotal role of RIPOR2 suggested by our data, we next sought potential small molecules that could target the RIPOR2 pathway and thereby counteract T cell exhaustion. Through molecular docking screens, we identified Ginsenoside F3 (GF3), a natural triterpene saponin from ginseng, as a candidate compound with high predicted affinity for RIPOR2. GF3 docked into the RIPOR2 protein with a binding energy of –9.6 kcal/mol (Fig. S5A, B), indicating a favorable and potentially specific interaction. To further validate the interaction between GF3 and RIPOR2, we performed surface plasmon resonance (SPR) experiments, which demonstrated a strong binding affinity of 3.77e-06 ±0.2 M between the two molecules(Fig. S5C). Given that ginsenosides are known to possess immunomodulatory properties, the strong docking score and SPR results suggested that GF3 might modulate RIPOR2 function or expression. Based on these findings, we hypothesized that GF3 could alleviate T cell exhaustion by targeting RIPOR2.

To test this hypothesis, we evaluated the effect of GF3 on T cell exhaustion *in vitro*. We added GF3 at various concentrations (0, 0.1, 1, 10 μM) to our chronic anti-CD3 stimulation cultures and monitored exhaustion markers over time. Flow cytometric analysis was performed on day 4 and day 6 of chronic stimulation to gauge how GF3 influences the differentiation of $CD8^+$ *T* cells into exhausted cells (experimental

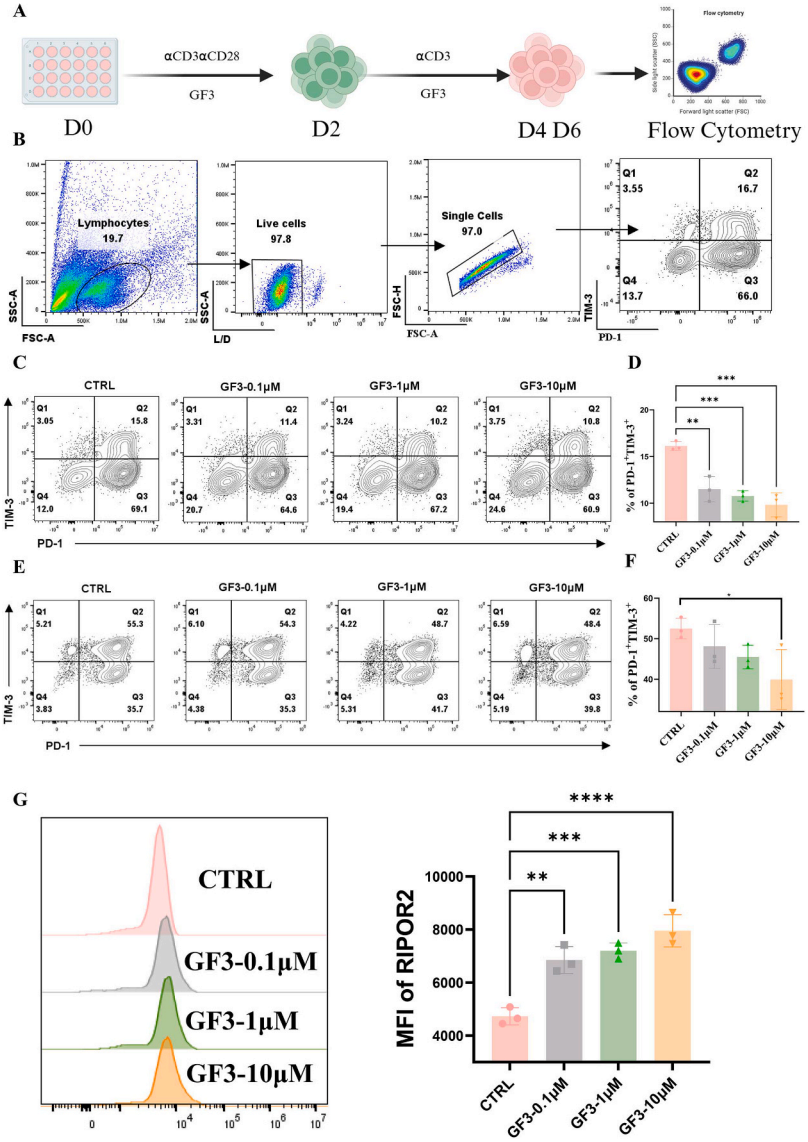

Fig. 3. Effect of GF3 intervention on T cell exhaustion differentiation A. Flowchart of GF3 intervention in T cell exhaustion. GF3 treatment was initiated at D0, followed by flow cytometry analysis at D4 and D6. B. Gating strategy for PD-1 and TIM-3 expression analysis in $CD8^+$ *T* cells by flow cytometry. C. PD-1 and TIM-3 expression in $CD8^+$ *T* cells after GF3 intervention (0, 0.1, 1, 10 μM) at D4. Data show one representative experiment. D. Statistical results of PD-1 and TIM-3 expression in $CD8^+$ *T* cells after GF3 interventionat D4 (0, 0.1, 1, 10 μM) ($n = 3$). E. PD-1 and TIM-3 expression in $CD8^+$ *T* cells after GF3 intervention (0, 0.1, 1, 10 μM) at D6. Data show one representative experiment. F. Statistical results of PD-1 and TIM-3 expression in $CD8^+$ *T* cells after GF3 interventionat D4 (0, 0.1, 1, 10 μM) ($n = 3$). G.Flow cytometry was used to detect the expression of RIPOR2 after GF3 intervention (0, 0.1, 1, 10 μM) ($n = 3$).

scheme in Fig. 3A). Remarkably, GF3 treatment mitigated the development of the exhausted phenotype in a dose-dependent manner. By day 4, the control group (no GF3) showed ~16.1 % of $CD8^+$ *T* cells co-expressing PD-1 and TIM-3. In contrast, all GF3-treated groups had a significantly lower percentage of $PD\text{-}1^+TIM\text{-}3^+$ cells: 11.5 ± 0.78 % with 0.1 μM GF3, 10.8 ± 0.32 % with 1 μM, and 9.8 ± 0.74 % with 10 μM (Fig. 3B–D). Even the lowest dose (0.1 μM) caused a noticeable reduction, and higher doses achieved a ~40 % reduction in exhausted subset frequency relative to control by day 4 ($p < 0.01$ for each GF3 dose *vs* control). This indicates that GF3 delays or suppresses the induction of terminal exhaustion during the early phase of chronic stimulation.

When we continued the chronic stimulation to day 6, we observed that GF3 continued to restrain exhaustion progression. In the absence of GF3, day 6 Tex cells exhibited very high inhibitory receptor expression (as shown earlier). GF3-treated cells, however, had lower surface levels of PD-1 and TIM-3, as measured by mean fluorescence intensity (MFI). Specifically, PD-1 MFI on $CD8^+$ *T* cells was reduced in GF3 groups compared to control (Fig. S6A). The decrease was significant for the 10 μM dose ($p < 0.05$ vs control). TIM-3 MFI showed an even more pronounced reduction with GF3, at 1 μM and 10 μM GF3, TIM-3 levels were substantially lower than in control (*$p < 0.01$; Fig. S6B). In terms of the fraction of fully exhausted ($PD\text{-}1^+TIM\text{-}3^+$) cells at day 6, the control group reached ~52.5 %, whereas GF3-treated groups showed a dose-dependent decline: 48.1 ± 3.12 % (0.1 μM), 45.5 ± 1.67 % (1 μM), and 39.9 ± 4.26 % (10 μM) (Fig. 3E, F). The highest dose of GF3 achieved the greatest reduction (~13 percentage points lower than control, $p < 0.05$). These data demonstrate that GF3 significantly curtails the accumulation of terminally exhausted T cells under chronic stimulation conditions. GF3-treated T cells maintain a more progenitor/effector-like phenotype, with fewer cells becoming $PD\text{-}1^{hi}TIM\text{-}3^{hi}$. This result is consistent with GF3 interfering in the exhaustion program, potentially *via* effects on RIPOR2 or downstream pathways.

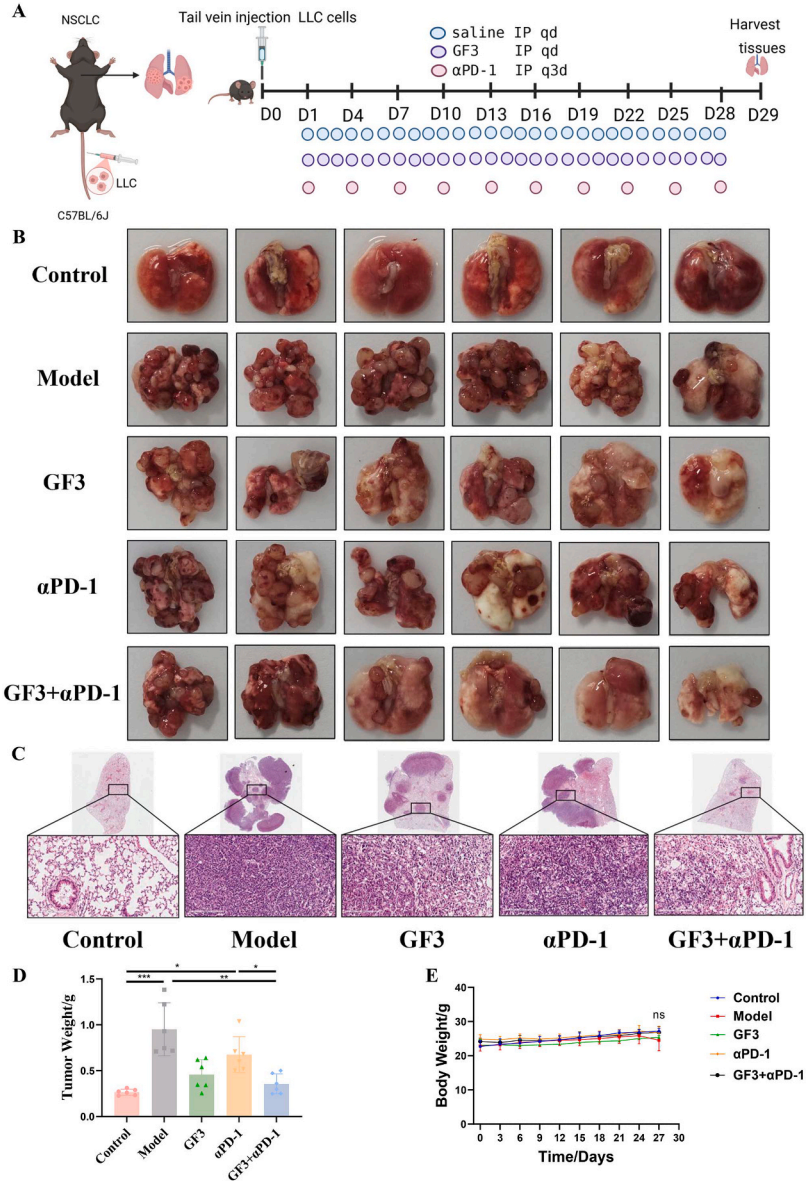

Fig. 4. *In vivo* study- GF3 synergizes with PD-1 blockers to alleviate NSCLC progression. A. Establishment of an orthotopic metastatic NSCLC model and therapeutic interventions *in vivo*. On day 0, LLC cells (4×10^5) were intravenously injected *via* tail vein into male C57BL/6 J mice (6–8 weeks old). Mice were divided into: 1) Control group(saline, i.p., daily, 100 μl), 2) Model group, 3) GF3 group (5 mg/kg, i.p., daily, 100 μl), 4) αPD-1 group (200 μg, i.p., every 3 days, 100 μl), (5) GF3+αPD-1 combination group receiving both treatments. Treatment was administered from Day 1 to Day 28. After 29 days of treatment, mice were euthanized by isoflurane anesthesia for tissue collection ($n = 6$). B. Lung tumor images from orthotopic implantation models across experimental groups. C. H&E staining results of lung tumors across experimental groups. D. Statistical results of lung tumor weight. E. The body weights of the mice in each group.

It is interesting to exame whether GF3 indeed influences RIPOR2 expression in T cells, as our hypothesis predicts. $CD8^+$ *T* cells were chronically stimulated with or without GF3 (at the same concentrations) and RIPOR2 mRNA was measured by qRT-PCR. Strikingly, GF3 treatment led to a dose-dependent upregulation of RIPOR2 transcripts in these T cells (Fig. S6C). Relative to the control group (set to 1.0), RIPOR2 expression increased to 2.12±0.08 with 0.1 μM GF3, 2.05±0.05 with 1 μM GF3, and 4.57±0.20 with 10 μM GF3 ($p < 0.001$ for all *vs* control). To further clarify the ability of GF3 to regulate RIPOR2, we used flow cytometry to detect the expression of RIPOR2 at the protein level in $CD8^+$*T* cells after GF3 intervention. The results showed that The expression of RIPOR2 was significantly enhanced after GF3 intervention ($p < 0.01$ for all *vs* control) (Fig. 3G). Thus, GF3 rescued or elevated the expression of RIPOR2 that is normally suppressed during chronic stimulation. This finding strongly supports our model, GF3 can target the RIPOR2 pathway, and its exhaustion-alleviating effects correlate with restoration of RIPOR2 levels in $CD8^+$ *T* cells.

Ginsenoside F3 synergizes with PD-1 blockade to suppress NSCLC tumor progression

We next evaluated whether GF3's pro-T cell effects could translate into improved tumor control, especially in synergy with PD-1 checkpoint inhibition. GF3 was administered at 5 mg/kg intraperitoneally, three times per week, and anti-PD-1 antibody at 200 μg per dose twice per week, based on regimens from prior studies. After 29 days of treatment, mice were euthanized for analysis (Fig. 4A). We found that GF3 enhances the efficacy of PD-1 blockade in controlling NSCLC tumor growth. In vehicle-treated tumor-bearing mice (Model group), the lungs were studded with numerous tumor nodules, and the lung weight was significantly increased due to tumor burden (0.907±0.137 g *vs* 0.266 ±0.013 g in healthy controls, $^{**}p < 0.001$; Fig. 4B, D). Histological examination (H&E staining) confirmed extensive tumor infiltration in the lungs of the Model group, with multiple dense nests of cancer cells exhibiting high nucleus-to-cytoplasm ratios (Fig. 4C). These findings verify successful establishment of aggressive lung tumors. Mice treated with anti-PD-1 monotherapy showed a modest reduction in tumor nodules and lung weight (mean 0.652±0.092 g), but this did not reach statistical significance *vs* the model (saline) group. Similarly, GF3 monotherapy yielded a lung tumor weight of 0.457±0.067 g – a trend towards improvement. Strikingly, the combination of GF3 + anti-PD-1 resulted in much better tumor control. Lungs from the combo group had visibly fewer and smaller tumor nodules (Fig. 4B), and the lung tumor weight was the lowest among all tumor-bearing groups (0.390 ±0.050 g). The combination group's tumor burden was significantly less than that of the Model group ($^*p < 0.01$) and also significantly less than the anti-PD-1 monotherapy group ($^*p < 0.05$; Fig. 4D). In fact, GF3 + anti-PD-1 brought the lung weight close to the level of healthy mice, indicating a near-complete suppression of tumor growth in some cases.

Histopathology corroborated these quantitative measurements. H&E-stained lung sections from the combination-treated mice revealed large areas of normal alveolar architecture with only occasional tumor foci, whereas the saline and monotherapy groups showed widespread tumor occupation (Fig. 4C). The combo group's remaining tumor cells appeared more scattered and less pleomorphic, with more evidence of tumor cell death. Overall, the GF3/PD-1 combo therapy dramatically inhibited NSCLC tumor progression, outperforming either agent alone. Importantly, throughout the treatment period, no significant weight loss or systemic toxicity was observed in any group (Fig. 4E). Mice in the GF3-treated groups maintained body weights similar to controls, suggesting that GF3 at the effective dose has no overt adverse effects. This lack of toxicity is encouraging for the potential therapeutic use of GF3.

To elucidate how GF3 augments anti-PD-1 therapy, we examined immune cell composition in the tumor microenvironment of treated mice. We focused on T lymphocytes, given that PD-1 therapy targets T cells and GF3 was designed to affect T cell exhaustion. We isolated mononuclear cells from digested lung tumors of each group and performed flow cytometry to quantify tumor-infiltrating T cell subsets. Gating on $CD3^+$ tumor-infiltrating lymphocytes, we measured the proportions of $CD4^+$T cells and $CD8^+$ *T* cells (Fig. 5A, B). In the *saline-treated Model* group, we found a relatively low baseline infiltration of T cells, typical of an immunosuppressive tumor. The percentage of $CD4^+$ *T* cells among $CD3^+$ TILs was around 19 %, and $CD8^+$ *T* cells around 20 % (Fig. 5C).

Treatment with GF3 alone led to a significant increase in the $CD4^+$ *T* cell fraction within tumors (28.1 ± 2.1 % *vs* 19.5 ± 3.9 % in model, $p < 0.05$; Fig. 5D). This suggests GF3 might help recruit or expand $CD4^+$ *T* cells (possibly including helper T cells) in the tumor milieu. Anti-PD-1 monotherapy did not significantly change $CD4^+$ TIL levels compared to model. Importantly, the $CD8^+$ *T* cell infiltration was markedly affected by the combination therapy. Neither GF3 alone (24.8 ± 2.1 %) nor PD-1 alone (24.6 ± 3.9 %) showed a statistically significant rise in $CD8^+$ TIL percentages, although there was a trend toward improvement. In contrast, the GF3 + PD-1 combination elicited a substantial increase in $CD8^+$ *T* cell representation among TILs (37.1 ± 1.9 %; $p < 0.05$ vs model and *vs* PD-1 alone; Fig. 5E). Thus, the combo therapy roughly doubled the proportion of intratumoral CD8 T cells compared to untreated tumors. This finding aligns perfectly with the notion that GF3 rescues exhausted $CD8^+$ *T* cells or facilitates their accumulation/maintenance in tumors, thereby amplifying the effect of PD-1 blockade. PD-1 blockade requires available T cells to rejuvenate; GF3 provides more and better-functioning T cells in the tumor for the antibody to act upon. The increased CD8 infiltration in the combo group correlates with its superior tumor control, highlighting that anti-tumor immunity was enhanced synergistically. Notably, the combo also maintained the elevated CD4 T cell levels seen with GF3 (the combo CD4 % was similar to GF3 alone, ~27–28 %), indicating that both helper and cytotoxic T cell compartments were improved. In summary, GF3 + anti-PD-1 therapy reprogrammed the TIL landscape, boosting especially the cytotoxic $CD8^+$ *T* cell presence in tumors.

GF3's anti-NSCLC efficacy is mediated by reinforcing $CD8^+$ T cell responses rather than direct tumor killing

While the above data strongly implicate an immune-mediated mechanism for GF3, we wanted to definitively distinguish whether GF3's anti-tumor effect was direct (tumor-cell cytotoxic) or indirect (immune-mediated). Many small molecules can have direct antiproliferative or pro-apoptotic effects on cancer cells. We therefore assessed GF3's direct toxicity on NSCLC cells *in vitro*. Two human NSCLC cell lines (H1299 and A549) and the murine LLC line were treated with a range of GF3 concentrations (0, 0.1, 1, 10, 100 μM), and cell viability was measured by CCK-8 assay after 48 h. The results showed that low-dose GF3 (≤10 μM) had no significant cytotoxic effect on any of the lung cancer cell lines (Fig. 6A–C). The viability curves for 0–10 μM were nearly flat, indicating that concentrations of GF3 achievable *in vivo* (likely in this low micromolar range given 5 mg/kg dosing) do not directly kill tumor cells. Only at a very high concentration (100 μM) did GF3 exhibit some inhibitory effect on the human NSCLC cells A549 and H1299 ($p < 0.05$ vs untreated; Fig. 6A, B). Even then, the effect was modest (perhaps ~20 % reduction in viability) and importantly, 100 μM GF3 had no significant impact on the viability of LLC cells (Fig. 6C). These data confirm that GF3 is not an effective direct anti-cancer agent at relevant doses – especially not against the mouse LLC cells used in our *in vivo* model, where we saw no toxicity. Therefore, the tumor suppression observed *in vivo* with GF3 is unlikely due to GF3 harming the cancer cells directly. This points toward an indirect anti-tumor mechanism, presumably by empowering the immune system (in particular, T cells) to attack the cancer.

We next investigated how GF3 influences T cells themselves, beyond simply reducing exhaustion markers. In addition to preventing dysfunction, an ideal immunotherapeutic agent might also promote T

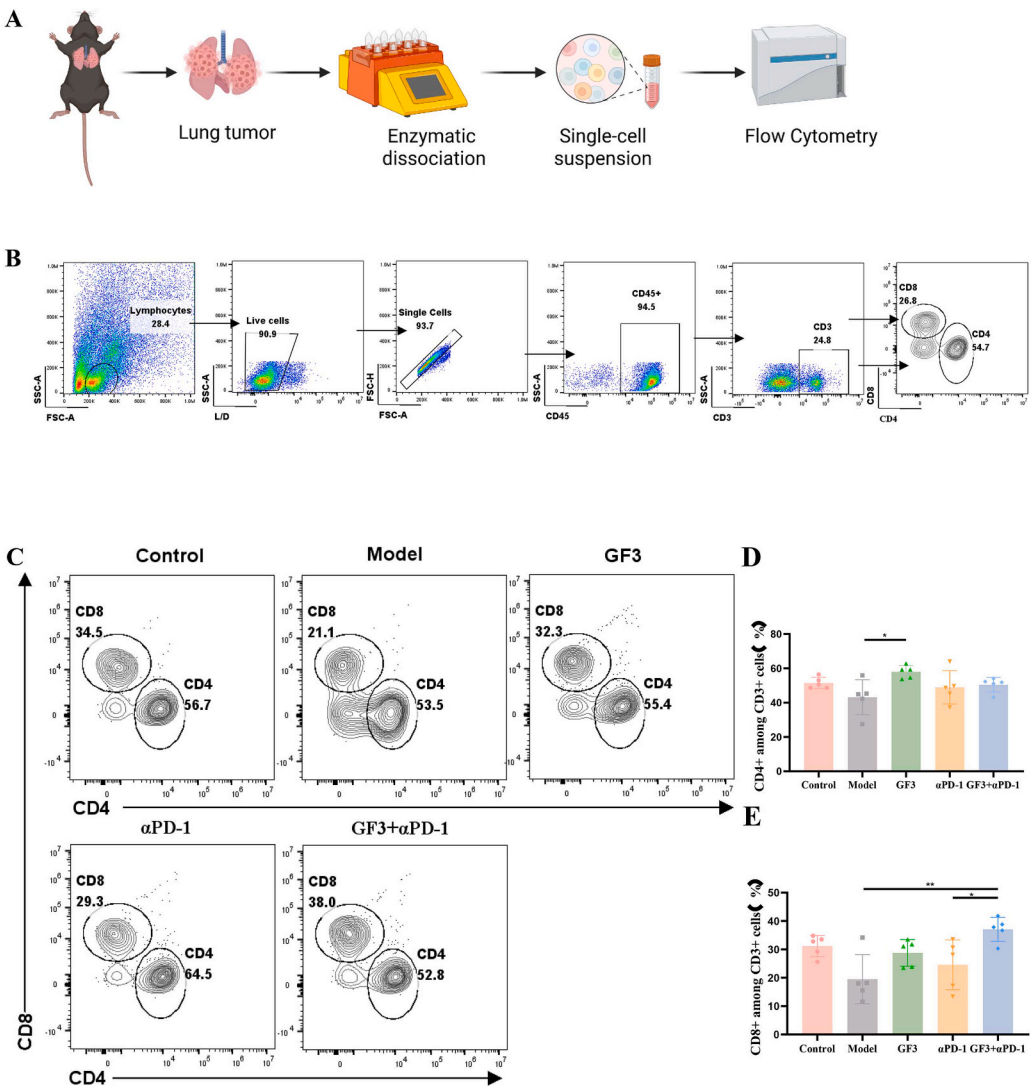

Fig. 5. CD4+/CD8+ *T* cell ratio in mouse tumor tissues A. Flow Cytometry Workflow for T Cell Proportion Analysis in Mouse Tumor Tissues. B. Gating Strategy for Flow Cytometry Analysis of Tumor-Infiltrating T Cells C. $CD4^+/CD8^+$T cell ratio in tumor tissues across experimental groups (representative experiment shown). D. Proportion of $CD4^+$ *T* cells across experimental groups (statistical results). E. Statistical results of $CD8^+$T cell proportions across experimental groups.

cell proliferation or survival. We examined the effect of GF3 on T cell growth using the Jurkat T cell line as a model for rapidly proliferating T cells. Jurkat cells were cultured with increasing doses of GF3 (0 to 100 μM) for 48 h, and cell proliferation was measured by CCK-8 assay. Interestingly, GF3 enhanced the proliferation of Jurkat T cells at certain doses (Fig. 6D). At 0.1 μM, there was a trend toward increased cell number (slightly above 100 % of control). Significant proliferative boosts were seen at 1 μM and 10 μM GF3 ($p < 0.05$ vs control), with the 10 μM dose showing the largest increase (about 20 % higher absorbance than control). The effect tapered off at 100 μM, where proliferation was still above control but less than at 10 μM (suggesting very high concentrations might be less beneficial, possibly due to minimal toxicity or feedback mechanisms). These results indicate that low-dose GF3 can act as a T cell stimulant, promoting T cell proliferation. This property would be advantageous in the context of immunotherapy, as it could expand the pool of effector T cells available to fight the tumor.

Then it is important to assess whether GF3 could functionally restore cytokine production in exhausted primary T cells, as hinted by our earlier *in vitro* findings. Mouse primary $CD8^+$ *T* cells were isolated and subjected them to the chronic stimulation exhaustion protocol, in the presence or absence of GF3. On day 6, we performed intracellular cytokine staining to measure the ability of these cells to produce *TNF-α* and *IFN-γ* upon restimulation (Fig. 6E). The results were striking: GF3-treated exhausted T cells exhibited a significant resurgence in effector cytokine production. The percentage of $CD8^+$ *T* cells co-expressing TNF-α and IFN-γ was only ~42.5 % in the exhausted control group (already higher than fully exhausted *in vivo* TILs, likely due to the acute restimulation *in vitro*). With GF3 treatment, this dual-cytokine-positive fraction rose dramatically – to 57.9 ± 1.51 % at 0.1 μM, 59.3 ± 2.39 % at 1 μM, and 60.4 ± 1.87 % at 10 μM (Fig. 6F). All these increases were highly significant (**$p < 0.001$ vs control), and they followed a dose-dependent trend. The 10 μM GF3 condition yielded the highest functional T cell fraction, consistent with it being the most effective dose for reducing exhaustion markers as well. In terms of overall cytokine output per cell, GF3 likewise improved performance. The MFI of TNF-α in GF3-treated T cells was elevated compared to control, with 10 μM GF3 causing a significant uptick in TNF-α levels (*$p < 0.01$; Fig. 6H). IFN-γ MFI saw an even larger boost: even the lowest GF3 dose increased IFN-γ intensity, and 1–10 μM GF3 raised IFN-γ MFI by ~2-fold or more relative to control (**$p < 0.001$; Fig. 6I). These data demonstrate that GF3 functionally rejuvenates exhausted T cells, restoring their capacity to secrete key effector cytokines. Essentially, GF3-treated "exhausted" T cells behave more like functional effector T cells in terms of cytokine secretion profile.

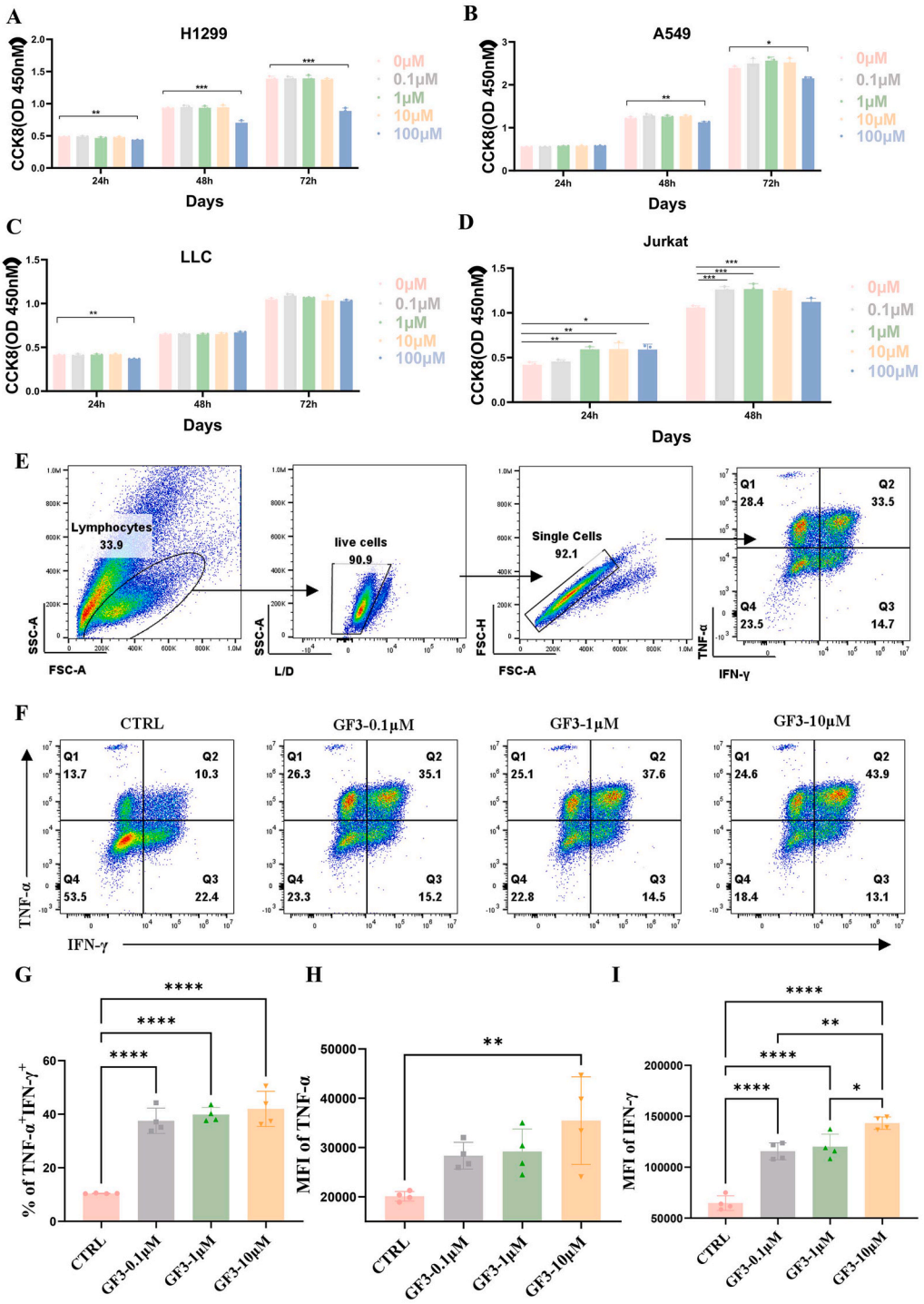

Fig. 6. GF3-mediated tumor cell cytotoxicity and modulation of CD8 T cell effector functions. A-D. H1299, A549, LLC and Jurkat cells were cultured in 0, 0.1, 1, 10 and 100 μM GF3 medium for 1–3 days, and then CCK8 reagent was incubated for 2 h—statistical plots of OD values at 450 nm ($n = 3$). E. Gating Strategy for Cytokine Secretion Analysis (TNF-α, IFN-γ) by Flow Cytometry F. Cytokine secretion profiles (TNF-α, IFN-γ) across experimental groups (representative experiment shown). G. Statistical results of cytokine secretion (TNF-α, IFN-γ) across experimental groups ($n = 3$). H. Statistical results of TNF-α MFI expression under GF3 intervention ($n = 3$). I. Statistical results of IFN-γ MFI expression under GF3 intervention ($n = 3$).

Discussion

T cell exhaustion is a pioneering area in anti-cancer practice attracting numerous researchers focusing on it. Our results identify RIPOR2 as a novel metabolic regulator of $CD8^+$ *T* cell exhaustion. Through proteomic screening of chronically stimulated T cells, we found that RIPOR2 expression is markedly reduced in exhausted $CD8^+$ *T* cells, suggesting its downregulation is associated with the terminal exhaustion state. Functionally, loss of RIPOR2 accelerated the progression to terminal exhaustion. T cells with RIPOR2 knockdown or deletion showed a higher frequency of *terminally exhausted* phenotypes (PD-1^{hi}TIM3^+TCF-1^{lo}) and a contraction of the TCF-1^+ progenitor-exhausted pool. Notably,

RIPOR2-deficient CD8$^+$ *T* cells lost the self-renewing TCF-1$^+$ progenitor subset – the population crucial for maintaining long-term responses(H. H. Wu et al., 2023). This was accompanied by diminished effector cytokine secretion (*e.g.*, IFN-γ, TNF-α), consistent with an exacerbation of the dysfunctional, "exhausted" state (Peralta et al., 2024). In contrast, restoring RIPOR2 expression helped preserve T cell functionality. We demonstrate that the small-molecule Ginsenoside F3 (GF3) upregulates RIPOR2 in exhausted T cells, thereby reinvigorating their function both *in vitro* and *in vivo*. GF3-treated CD8$^+$ *T* cells reduced the proportion of terminally exhausted T cells (PD-1^{hi}TIM3$^+$) and produced higher levels of effector cytokines compared to untreated exhausted T cells. In tumor-bearing mice, GF3 therapy alleviated T cell exhaustion and enhanced anti-tumor immunity, leading to improved clearance of tumors especially when combined with PD-1 checkpoint blockade. Strikingly, GF3-treated mice receiving anti-PD-1 showed synergistic tumor control, with slower tumor growth and prolonged survival relative to PD-1 blockade alone (Fig. 7). These results position RIPOR2 as a critical checkpoint in the exhaustion trajectory, and GF3 as a promising agent to restore T cell metabolic fitness and function during chronic antigen exposure.

Exhausted T cells often exhibit a metabolic switch (for instance, reduced glycolytic capacity and mitochondrial defects) that impairs their function. Our data reinforce the concept that metabolic regulators are closely linked to the exhausted phenotype, and targeting metabolic pathways might modulate exhaustion (de la Cruz-López et al., 2019). Hypoxia and nutrient competition in tumors can promote T cell exhaustion, suggesting that relieving metabolic stress (*e.g.* by blocking lactic acid uptake) might restore T cell activity (Fischer et al., 2007). Indeed, a recent study showed that terminally exhausted T cells upregulate MCT11, a lactate transporter, and blocking lactate utilization reinvigorated T cells and reduced tumor growth in mice. Strategies to "reprogram" T cell metabolism – such as enhancing oxidative metabolism or inhibiting tumor glycolysis – are now recognized as promising ways to mitigate exhaustion and improve immunotherapy. Metabolic modulators (for instance, IDO1 inhibitors targeting the tryptophan pathway, or adenosine A2A receptor antagonists targeting the adenosine pathway) are being explored in combination with ICIs, although clinical success has been limited so far (*e.g.* the IDO inhibitor epacadostat failed to improve outcomes in melanoma when added to anti-PD-1 therapy) (Agarwala et al., 2024).

Our previous studies demonstrated that ceramide synthase 4 (CERS4) modulates RHO family proteins to reshape the tumor immune microenvironment, thereby alleviating T cell exhaustion and enhancing the efficacy of PD-1 monoclonal antibody therapy in NSCLC (Wang

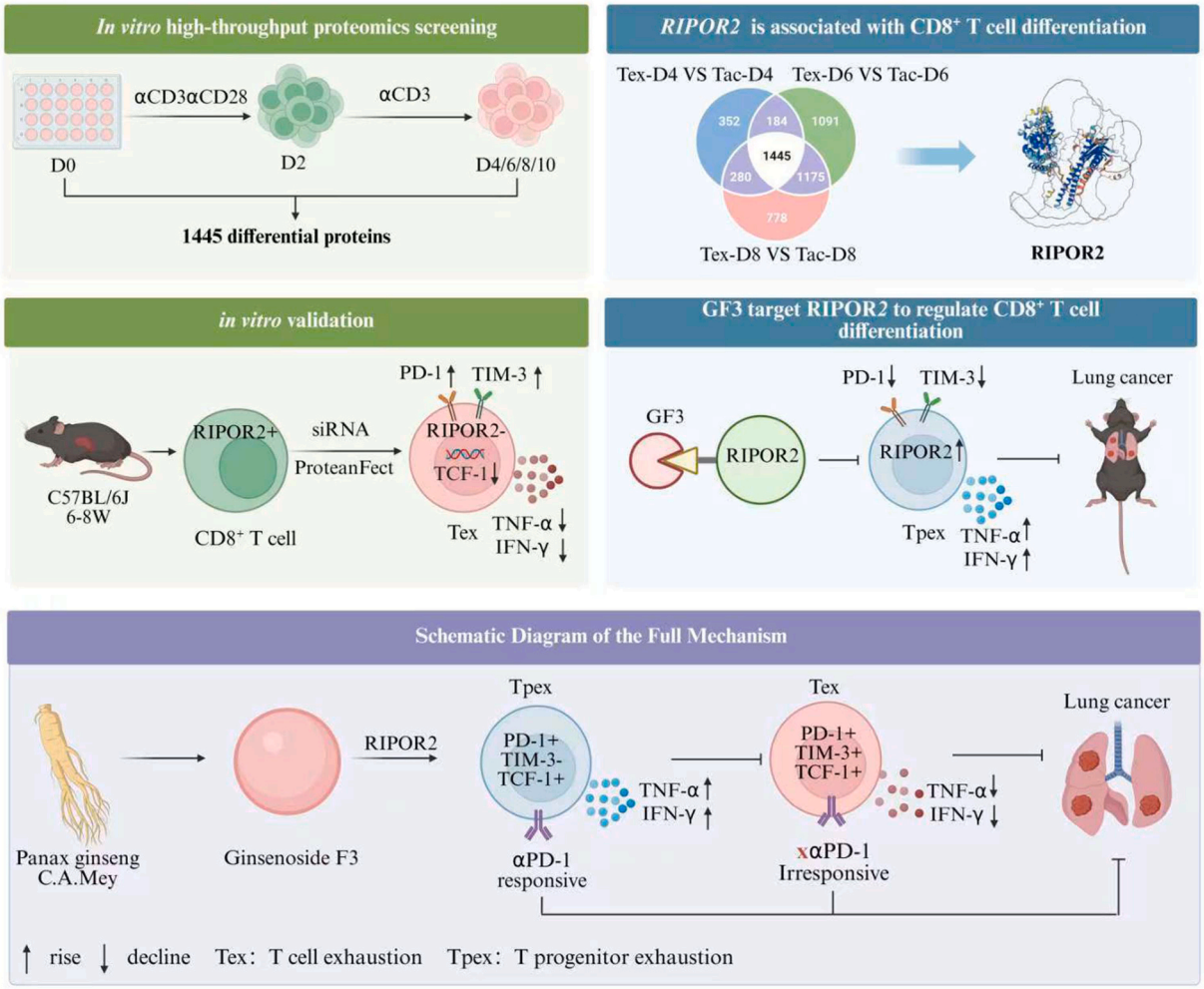

Fig. 7. Potential mechanism of Ginsenoside F3 in alleviating T cell exhaustion and synergizing with anti-PD-1 therapy in NSCLC. Specifically, an *in vitro* T cell exhaustion model was established *via* chronic anti-CD3 stimulation. Time-course proteomic profiling of this model identified the progressive down-regulation of RIPOR2 as a critical event linked to the loss of T cell stemness and function. Then, molecular docking revealed that Ginsenoside F3 (GF3), a compound derived from Panax ginseng C.A.Mey, can target the RIPOR2. After intervention with Ginsenoside F3, the proportion of PD-1+ TIM-3+ CD8+ T cells decreased, while the ability to secrete cytokines (TNF-α, IFN-γ) improved. Additionally, GF3 restored PD-1 blockade sensitivity in previously resistant T cells, and its combination with PD-1 blockade synergistically improved therapeutic efficacy against NSCLC.

et al., 2023). Our proteomic data further revealed that RIPOR2 plays a critical role in maintaining T cell function and mitigating T cell exhaustion progression. Notably, RIPOR2 may inhibit RhoA activity in cells and is functionally associated with T cell proliferation, differentiation, and migration (Jeanne Froehlich, 2016; Megrelis et al., 2018; Rougerie et al., 2013). Our findings highlight RIPOR2 as a regulator of T cell exhaustion distinct from the canonical transcriptional factors (TOX, NR4A, BATF) that have been previously described. .RIPOR2 appears to operate through immunometabolic pathways rather than direct gene transcription. RIPOR2 has not been implicated in chromatin remodeling; instead, our data suggest it influences the metabolic state and signaling milieu of T cells during chronic stimulation. Notably, RIPOR2 downregulation led to bioenergetic defects characteristic of exhausted T cells (such as poor mitochondrial maintenance and low cytokine output), indicating a link to cellular metabolism. This aligns with emerging evidence that metabolic stress is a key driver of T cell exhaustion alongside transcriptional programs (Scharping et al., 2021). Recent studies have shown that nutrient-deprived, hypoxic tumor microenvironments (TME) can accelerate T cell dysfunction even in the presence of continued antigen stimulation. For instance, terminally exhausted T cells upregulate the monocarboxylate transporter MCT4/Slc16a11 and take up excess lactic acid in tumors, which impairs their function; blocking this lactate uptake reinvigorates T cells and improves tumor control (Peralta et al., 2024). Similarly, mitochondrial insufficiency and redox stress can initiate an exhaustion program *via* HIF-1α stabilization and glycolytic skewing (Scharping et al., 2021). In this context, RIPOR2's role as a metabolic regulator is distinct: rather than dictating the epigenetic identity of exhausted T cells, RIPOR2 modulates pathways like cytoskeletal dynamics and cellular metabolism (potentially glucose uptake or mitochondrial positioning) that ultimately impact T cell longevity and cytokine secretion. By targeting RIPOR2, GF3 intervenes at this metabolic–signaling nexus – in effect, rebalancing the T cell's metabolic fitness to prevent or reverse exhaustion. This mechanism contrasts with approaches aimed at TOX or NR4A, which would alter transcriptional programs; instead, RIPOR2 enhancement *via* GF3 bolsters the cell's metabolic infrastructure, thereby supporting the progenitor pool and effector functions without directly editing the genome-wide exhaustion profile. Our study therefore broadens the paradigm of T cell exhaustion regulation, introducing metabolic regulators like RIPOR2 as complements to the well-known transcription factors in controlling T cell fate.

Chronic stimulation with anti-CD3 antibodies to construct T cell exhaustion has unique advantages. Our *in vitro* T cell exhaustion model offers a scalable, reductionist system to study chronic stimulation and test interventions, and we contrast it with traditional *in vivo* models such as chronic LCMV infection and tumor-infiltrating lymphocyte (TIL) analyses. Classic models like the LCMV clone-13 chronic infection in mice have been instrumental in defining exhaustion but are logistically complex and limited in throughput. They recapitulate antigen persistence and T cell dysfunction *in vivo*, yet interventional testing (*e.g.*, multiple small molecules) can be slow and confounded by systemic factors. By contrast, our *in vitro* model induces exhaustion under controlled conditions – continuous TCR stimulation with defined metabolic stresses – enabling reproducible expansion of "exhausted" T cells for mechanistic assays and drug screening. Consistent with other recent *in vitro* approaches, we observed that TCR stimulation alone was not sufficient to drive full exhaustion unless coupled with metabolic/environmental stress. In our system, we mimicked TME-like stress (*e.g.* nutrient limitation or accumulated inhibitory metabolites) alongside chronic antigenic stimulation. This approach is analogous to the method of Scharping et al. (2021), who showed that continuous TCR triggering under hypoxia rapidly drives an exhausted-like state *in vitro*, whereas TCR triggering in normoxia yields functional effectors (Scharping et al., 2021). Similarly, other groups have induced T cell dysfunction *in vitro* using glucose deprivation or high lactic acid conditions, replicating the nutrient competition and lactic acidosis of tumors that enforce T cell exhaustion (Gu et al., 2025). Such models are highly scalable and tunable, allowing precise timing of interventions like GF3 addition at different stages of exhaustion.

Compared to TIL-based models (analyzing endogenous tumor-infiltrating T cells ex vivo), our approach allows earlier and more homogeneous induction of exhaustion, simplifying interpretation of how a compound affects "pre-exhausted" *versus* terminally exhausted cells. While TIL analyses provide authentic tumor context, they often yield a mix of T cell states and are low-throughput. Our *in vitro* exhausted T cells exhibit hallmark features (PD-1^{hi}, Tim-3^{+}, reduced cytokines), paralleling the phenotypes seen *in vivo* (Multhoff et al., 2014). Importantly, we validated our *in vitro* findings in an *in vivo* tumor setting, where GF3 treatment mirrored the *in vitro* results by sustaining progenitor Tex cells and improving function in the TME. This demonstrates that while simplified, the *in vitro* model is relevant to physiological exhaustion and suitable for preclinical testing of interventions. That said, each model has merits: LCMV chronic infection remains a gold-standard for studying exhaustion development and reversal (*e.g.*, with checkpoint blockade) in an intact immune system (Zehn et al., 2022). Our results complement these by providing an orthogonal strategy (metabolic reprogramming *via* RIPOR2) that could be applied to TIL expansion to retain more stem-like, less exhausted T cells. In summary, our *in vitro* model's strength lies in scalability and controllability, making it an efficient testbed for compounds like GF3, whereas *in vivo* models ensure that findings translate in the context of whole-organism biology. We leveraged both: first establishing GF3's efficacy *in vitro*, then confirming *in vivo* synergy with PD-1 blockade, thereby underscoring the translational potential of our findings.

Tumor immune escape involves multiple pathways, and single-agent checkpoint blockade often falls short due to compensatory mechanisms. Therefore, multi-target combinations and multitargeted agents are gaining prominence. Unlike monoclonal antibodies which typically block a single extracellular target, small molecules offer unique advantages in fine-tuning the tumor immune microenvironment. They can be orally administered, diffuse into tumor sites, and target intracellular regulators that antibodies cannot. For example, small-molecule immunomodulators such as lenvatinib (a multikinase inhibitor) combined with anti-PD-1 have shown synergistic efficacy in hepatocellular carcinoma by simultaneously normalizing tumor vasculature and enhancing T cell infiltration. For instance, inhibiting the adenosine pathway with small-molecule A2A receptor antagonists or blocking lactate export with an MCT1 inhibitor (AZD3965) can relieve immunosuppression and boost $CD8^{+}$ *T* cell activity in tumors (Xu et al., 2025). Several small-molecule agents are in clinical trials as *immunotherapy adjuvants*, but truly effective "sensitizer" drugs have yet to be realized in practice.

Our study introduces Ginsenoside F3 (GF3) – a triterpenoid saponin from *Panax* ginseng – as a potent immunometabolic modulator that rescues T cell exhaustion. GF3's mechanism appears multifaceted: by restoring RIPOR2 levels, it improves metabolic fitness and cytokine production in exhausted T cells, thus operating at the intersection of immune signaling and cellular metabolism. It is instructive to compare GF3's profile with other metabolic interventions known to enhance T cell function. (1) Metformin (AMPK activator): A well-known antidiabetic drug, metformin has been repurposed in immuno-oncology for its T cell effects. Metformin improves $CD8^{+}$ *T* cell responses partly by relieving tumor hypoxia and metabolic stress. Metformin treatment in tumor models has been shown to reduce the population of PD-1^{hi} exhausted $CD8^{+}$ TILs and restore their effector activity, leading to enhanced responses to PD-1 checkpoint therapy (Abdelmoneim et al., 2023). This parallels GF3's ability to diminish exhaustion markers and boost cytokine secretion, though *via* a different molecular target. Metformin broadly activates metabolic checkpoints (AMPK) and encourages fatty-acid oxidation and mitochondrial function, whereas GF3 specifically upregulates RIPOR2 and downstream pathways. Both, however, converge on improving the energetic and redox state of T cells, thereby reviving their function in tumors. (2) CPI-613 (devimistat): This first-in-class lipoate analog inhibits the pyruvate dehydrogenase

complex, targeting tumor cell TCA cycle metabolism. In the context of immunity, CPI-613 represents a strategy to reprogram cellular metabolism in the tumor milieu. By inhibiting cancer cell oxidative metabolism and altering nutrient availability, CPI-613 can indirectly favor T cell activity; for instance, it was shown to increase $CD8^+$ *T* cell cytotoxicity and IFN-γ production in a tumor co-culture model (Kim et al., 2025). While GF3 does not directly inhibit tumor metabolism, it metabolically empowers T cells themselves. Thus, GF3 could potentially complement agents like CPI-613: one reduces tumor metabolic competition, the other fortifies T cell metabolic capacity. (3) IDO1 (indoleamine-2,3-dioxygenase) Inhibitors: IDO1 depletes tryptophan in the TME, blunting T cell proliferation and inducing a state resembling exhaustion/anergy. Small-molecule IDO1 inhibitors (*e.g.*, epacadostat) were developed to counteract this immunosuppressive metabolic pathway. Preclinical studies demonstrated that blocking IDO1 can boost T cell activity and synergize with PD-1 blockade, resulting in better tumor control than checkpoint therapy alone (Guangzhao et al., 2025). However, clinical trials of IDO1 inhibitors yielded mixed outcomes, partly due to compensatory mechanisms in human tumors. GF3 differs in that it directly targets the T cells' intrinsic machinery (RIPOR2) rather than the tumor or myeloid suppressive pathways. Thus, GF3 may provide benefits even in cases where tumor-derived metabolic suppression (like IDO-mediated tryptophan loss) is not the dominant factor – by making T cells intrinsically more resilient to chronic stimulation and nutrient stress.

A key advantage of GF3 is its natural origin and favorable safety profile. Ginsenosides (including F3) are bioactive compounds found in Panax ginseng C.A.Mey, an herbal medicine with centuries of human use. They are generally well-tolerated: ginseng extracts are considered safe and largely non-toxic in both animals and humans at recommended doses (Chang et al., 2003; Coon and Ernst, 2002). While pharmaceuticals like metformin or CPI-613 have their own safety data (metformin is widely used with mild side effects, CPI-613 is still under clinical evaluation for toxicity), GF3's natural derivation *a priori* suggests low systemic toxicity and the possibility of chronic administration (Mancuso and Santangelo, 2017). This is particularly important for exhaustion reversal, as treatments may need to be given over extended periods (to coincide with ongoing antigen exposure or alongside multiple cycles of immunotherapy). GF3's multi-target action could also be an asset: rather than inhibiting a single enzyme or receptor, it may exert a broad normalizing effect on T cell metabolism and signaling, which might reduce the chances of resistance (Lee and Son, 2011). That said, multi-target natural compounds require careful mechanistic dissection to ensure no off-target immune suppression occurs; our data so far indicate GF3's net effect is stimulatory, enhancing *both* the TCF-1^+progenitor pool and the terminal effector functions of CD8 T cells.

While our findings are encouraging, we recognize several limitations in the current study that should be addressed in future research. First, the pharmacokinetic and bioavailability profile of GF3 is not yet well characterized. Like many ginsenosides, GF3 may have poor oral absorption and rapid metabolism, which could limit its effectiveness *in vivo* (Won et al., 2019).Our experimental results also showed similar findings. Compared with low-dose GF3, high-dose GF3 did not exhibit significant dose-dependence (Fig.S7)., Hence, further work is needed to optimize its formulation or explore analogs for better systemic exposure. Improving GF3's bioavailability (through nanoparticle delivery, prodrug design, or formulation with absorption enhancers) will be crucial before any clinical translation. Second, our experiments were performed largely in murine systems – murine T cell lines *in vitro* and mouse tumor models *in vivo*. We have yet to confirm that GF3 can similarly rejuvenate human primary $CD8^+$ *T* cells. Human T cells may differ in RIPOR2 regulation or drug uptake; therefore, validation using human T cells from donors (for example, inducing exhaustion in human T cells with chronic stimulation and testing GF3 rescue) is a priority. In addition, it will be informative to assess GF3 in more complex humanized models or *ex vivo* human tumor organoid–T cell co-cultures, which better recapitulate the human TME. No organoid or 3D tissue models were used in this initial study, representing an area to expand upon to ensure that GF3's benefits are maintained in a setting with human tumor stroma, myeloid cells, and other factors present.

In conclusion, our work opens several avenues for future research. Confirming GF3's action in human T cells and improving its delivery will be key steps toward clinical translation. Additionally, exploring GF3 in combination with other therapies – beyond PD-1 blockade, perhaps with metabolic adjuvants or other checkpoint inhibitors – could capitalize on its immunometabolic modulation to achieve deeper or broader immune reinvigoration. Despite the limitations, our study provides a proof-of-concept that targeting metabolic regulators like RIPOR2 can reverse T cell exhaustion. This not only broadens the mechanistic understanding of exhaustion but also suggests a novel therapeutic strategy, positioning GF3 (and related compounds) as promising adjuncts to current immunotherapies. With further optimization and validation, GF3 or its derivatives could emerge as a clinically valuable tool to enhance T cell-mediated immunity in chronic infections and cancer, complementing the arsenal of immune checkpoint inhibitors and metabolic modulators in the fight against refractory disease.Based on our findings, we plan to employ CRISPR technology to knock down RIPOR2 in T cells and conduct transcriptomic and metabolomic studies to further elucidate the key molecular mechanisms by which RIPOR2 regulates T cell exhaustion.Additionally, we intend to validate our conclusions by investigating the effects of RIPOR2 protein and GF3 in various mouse tumor models. We also plan to initiate clinical studies focusing on immunotherapy non-responders, which will lay the foundation for the clinical translation of RIPOR2 as a therapeutic target and GF3 as a small molecule agent in tumor immunotherapy.

Conclusion

In summary, this study demonstrates that RIPOR2 serves as a critical regulator limiting T cell exhaustion. Targeting RIPOR2 may alleviate the progression of T cell exhaustion and restore the effector function of CD8+ *T* cells. Notably, ginsenoside F3, a bioactive small-molecule compound derived from traditional Chinese medicine with high binding affinity to RIPOR2, effectively mitigates T cell exhaustion and enhances T cell effector function. When combined with PD-1 blockade therapy, ginsenoside F3 synergistically suppresses non-small cell lung cancer (NSCLC) progression, offering a novel therapeutic strategy for NSCLC immunotherapy. Additionally, we employed an established *in vitro* T cell exhaustion model (induced by chronic CD3 antibody stimulation, as described in prior studies) to investigate the mechanisms of T cell exhaustion and evaluate drug efficacy. This model provides a reliable platform for mechanistic studies and therapeutic screening.

Data availability

The transcriptomic and single-cell RNA sequencing data generated and analyzed in this study are available at the National Center for Biotechnology Information (NCBI), and other data will be provided upon request.

Acknowledgments

This work was financially supported by a grant from the Non-communicable Chronic Diseases-National Science and Technology Major Project (2024ZD0521405), National Natural Science Foundation of China (82,204,677, 82,474,267), Major Project of Guangzhou National Laboratory(No. GZNL2023A02009), Traditional Chinese Medicine Bureau of Guangdong Province Project (NO. 20,241,112), State Key Laboratory of Traditional Chinese Medicine Syndrome (QZ2023ZZ11), Chinese Medicine Guangdong Laboratory (HQL2024PZ005, HQL2025CY007). We thank BioRender (biorender.com) for providing tools to create scientific figures in this paper.

Author agreement statement

We the undersigned declare that this manuscript is original, has not been published before and is not currently being considered for publication elsewhere.

We confirm that the manuscript has been read and approved by all named authors and that there are no other persons who satisfied the criteria for authorship but are not listed. We further confirm that the order of authors listed in the manuscript has been approved by all of us.

We understand that the Corresponding Author is the sole contact for the Editorial process.

He/she is responsible for communicating with the other authors about progress, submissions of revisions and final approval of proofs

CRediT authorship contribution statement

Menglin Jiang: Writing – original draft, Visualization, Formal analysis, Data curation. **Weiqian Bao:** Project administration, Data curation, Conceptualization. **Lewei He:** Visualization, Formal analysis, Data curation. **Yichun Liang:** Investigation, Formal analysis. **Nanjie Zhou:** Formal analysis, Data curation. **Cuifen Zhang:** Investigation, Data curation. **Yuanyuan Song:** Software, Formal analysis. **Gangyuan Ma:** Methodology. **Liqing Chen:** Data curation. **Kaoling Wen:** Data curation. **Yicheng Zhao:** Writing – review & editing. **Liang Liu:** Supervision, Project administration. **Hudan Pan:** Supervision, Project administration. **Runze Li:** Writing – review & editing, Supervision, Funding acquisition, Conceptualization.

Declaration of competing interest

The authors declare that they have no known competing financial interests or personal relationships that could have appeared to influence the work reported in this paper.

Supplementary materials

Supplementary material associated with this article can be found, in the online version, at doi:10.1016/j.phymed.2025.157649.

References

Abdelmoneim, M., Aboalela, M.A., Naoe, Y., Matsumura, S., Eissa, I.R., Bustos-Villalobos, I., Sibal, P.A., Takido, Y., Kodera, Y., Kasuya, H., 2023. The Impact of Metformin on Tumor-Infiltrated Immune Cells: preclinical and Clinical Studies. Int. J. Mol. Sci. 24 (17). https://doi.org/10.3390/ijms241713353.

Agarwala, Y., Brauns, T.A., Sluder, A.E., Poznansky, M.C., Gemechu, Y., 2024. Targeting metabolic pathways to counter cancer immunotherapy resistance. Trends. Immunol. 45 (7), 486–494. https://doi.org/10.1016/j.it.2024.05.006.

Belk, J.A., Yao, W., Ly, N., Freitas, K.A., Chen, Y.-T., Shi, Q., Valencia, A.M., Shifrut, E., Kale, N., Yost, K.E., Duffy, C.V., Daniel, B., Hwee, M.A., Miao, Z., Ashworth, A., Mackall, C.L., Marson, A., Carnevale, J., Vardhana, S.A., Satpathy, A.T., 2022. Genome-wide CRISPR screens of T cell exhaustion identify chromatin remodeling factors that limit T cell persistence. Cancer Cell 40 (7), 768–786. https://doi.org/10.1016/j.ccell.2022.06.001 e767.

Chang, Y.S., Seo, E.-K., Gyllenhaal, C., Block, K.I., 2003. Panax ginseng: a Role in Cancer Therapy? Integr. Cancer Ther. 2 (1), 13–33. https://doi.org/10.1177/1534735403251167.

Cheng, J., Xiao, Y., Peng, T., Zhang, Z., Qin, Y., Wang, Y., Shi, J., Yan, J., Zhao, Z., Zheng, L., He, Z., Wang, J., Zhang, Z., Li, C., Zhu, H., Jiang, P., 2025. ETV7 limits the antiviral and antitumor efficacy of CD8+ T cells by diverting their fate toward exhaustion. Nat. Cancer 6 (2), 338–356. https://doi.org/10.1038/s43018-024-00892-0.

Chow, A., Perica, K., Klebanoff, C.A., Wolchok, J.D., 2022. Clinical implications of T cell exhaustion for cancer immunotherapy. Nat. Rev. Clin. Oncol. 19 (12), 775–790. https://doi.org/10.1038/s41571-022-00689-z.

Coon, J.T., Ernst, E., 2002. Panax ginseng. Drug Saf. 25 (5), 323–344. https://doi.org/10.2165/00002018-200225050-00003.

de la Cruz-López, K.G., Castro-Muñoz, L.J., Reyes-Hernández, D.O., García-Carrancá, A., Manzo-Merino, J., 2019. Lactate in the regulation of tumor microenvironment and therapeutic approaches. In: Front. Oncol., 9. https://doi.org/10.3389/fonc.2019.01143.

Fagerberg, E., Attanasio, J., Dien, C., Singh, J., Kessler, E.A., Abdullah, L., Shen, J., Hunt, B.G., Connolly, K.A., De Brouwer, E., He, J., Iyer, N.R., Buck, J., Borr, E.R., Damo, M., Foster, G.G., Giles, J.R., Huang, Y.H., Tsang, J.S., Joshi, N.S., 2025. KLF2 maintains lineage fidelity and suppresses CD8 T cell exhaustion during acute LCMV infection. Science 1979 387 (6735). https://doi.org/10.1126/science.adn2337.

Fischer, K., Hoffmann, P., Voelkl, S., Meidenbauer, N., Ammer, J., Edinger, M., Gottfried, E., Schwarz, S., Rothe, G., Hoves, S., Renner, K., Timischl, B., Mackensen, A., Kunz-Schughart, L., Andreesen, R., Krause, S.W., Kreutz, M., 2007. Inhibitory effect of tumor cell–derived lactic acid on human T cells. Blood 109 (9), 3812–3819. https://doi.org/10.1182/blood-2006-07-035972.

Gu, X.-Y., Yang, J.-L., Lai, R., Zhou, Z.-J., Tang, D., Hu, L., Zhao, L.-J., 2025. Impact of lactate on immune cell function in the tumor microenvironment: mechanisms and therapeutic perspectives. Front. Immunol. 16. https://doi.org/10.3389/fimmu.2025.1563303.

Guangzhao, L., Xin, W., Miaoqing, W., Wenjuan, M., Ranyi, L., Zhizhong, P., Rongxin, Z., Gong, C., 2025. IDO1 inhibitor enhances the effectiveness of PD-1 blockade in microsatellite stable colorectal cancer by promoting macrophage pro-inflammatory phenotype polarization. Cancer Immunol., Immunother. 74 (2). https://doi.org/10.1007/s00262-024-03925-w.

Guo, X., Zhang, Y., Zheng, L., Zheng, C., Song, J., Zhang, Q., Kang, B., Liu, Z., Jin, L., Xing, R., Gao, R., Zhang, L., Dong, M., Hu, X., Ren, X., Kirchhoff, D., Roider, H.G., Yan, T., Zhang, Z., 2018. Global characterization of T cells in non-small-cell lung cancer by single-cell sequencing. Nat. Med. 24 (7), 978–985. https://doi.org/10.1038/s41591-018-0045-3.

Huang, J., Liu, D., Wang, Y., Liu, L., Li, J., Yuan, J., Jiang, Z., Jiang, Z., Hsiao, W.L.W., Liu, H., Khan, I., Xie, Y., Wu, J., Xie, Y., Zhang, Y., Fu, Y., Liao, J., Wang, W., Lai, H., Leung, E.L.-H., 2022. Ginseng polysaccharides alter the gut microbiota and kynurenine/tryptophan ratio, potentiating the antitumour effect of antiprogrammed cell death 1/programmed cell death ligand 1 (anti-PD-1/PD-L1) immunotherapy. Gut 71 (4), 734–745. https://doi.org/10.1136/gutjnl-2020-321031.

Huang, M.-Y., Chen, Y.-C., Lyu, W.-Y., He, X.-Y., Ye, Z.-H., Huang, C.-Y., He, X.-L., Chen, X., Chen, X., Zhang, B., Kai, G., Zhang, X., Li, T., Huang, M., Lu, J.-J., 2023. Ginsenoside Rh2 augmented anti-PD-L1 immunotherapy by reinvigorating CD8+ T cells *via* increasing intratumoral CXCL10. Pharmacol. Res. 198. https://doi.org/10.1016/j.phrs.2023.106988.

Jeanne Froehlich, M.V., Megrelis, L., Largeteau, Q., Meunier, S., Tanchot, C., Bismuth, G., Delon, J., Mangeney, M., 2016. FAM65B controls the proliferation of transformed and primary T cells. Oncotarget.

Jenkins, E., Whitehead, T., Fellermeyer, M., Davis, S.J., Sharma, S., 2023. The current state and future of T-cell exhaustion research. Oxf. Open. Immunol. 4 (1). https://doi.org/10.1093/oxfimm/iqad006.

Jiang, Y., Li, Y., Zhu, B., 2015. T-cell exhaustion in the tumor microenvironment. Cell Death. Dis. 6 (6), e1792. https://doi.org/10.1038/cddis.2015.162. -e1792.

Kang, T.G., Lan, X., Mi, T., Chen, H., Alli, S., Lim, S.-E., Bhatara, S., Vasandan, A.B., Ward, G., Bentivegna, S., Jang, J., Spatz, M.L., Han, J.-H., Schlotmann, B.C., Jespersen, J.S., Derenzo, C., Vogel, P., Yu, J., Baylin, S., Zebley, C.C., 2024. Epigenetic regulators of clonal hematopoiesis control CD8 T cell stemness during immunotherapy. Science 1979 386 (6718). https://doi.org/10.1126/science.adl4492.

Kim, J., Li, J., Wei, J., Lim, S.A., 2025. Regulatory T cell metabolism: a promising therapeutic target for cancer treatment? Immune Netw. 25 (1). https://doi.org/10.4110/in.2025.25.e13.

Lee, N.-H., Son, C.-G., 2011. Systematic review of randomized controlled trials evaluating the efficacy and safety of Ginseng. J. Acupunct. Meridian. Stud. 4 (2), 85–97. https://doi.org/10.1016/s2005-2901(11)60013-7.

Ma, K., Xu, Y., Cheng, H., Tang, K., Ma, J., Huang, B., 2025. T cell-based cancer immunotherapy: opportunities and challenges. Sci. Bulletin 70 (11), 1872–1890. https://doi.org/10.1016/j.scib.2025.03.054.

Mancuso, C., Santangelo, R., 2017. Panax ginseng and Panax quinquefolius: from pharmacology to toxicology. Food Chem. Toxicol. 107, 362–372. https://doi.org/10.1016/j.fct.2017.07.019.

Megrelis, L., El Ghoul, E., Moalli, F., Versapuech, M., Cassim, S., Ruef, N., Stein, J.V., Mangeney, M., Delon, J., 2018. Fam65b phosphorylation relieves tonic RhoA inhibition during T cell migration. Front. Immunol. 9. https://doi.org/10.3389/fimmu.2018.02001.

Mortazavi Farsani, S.S., Soni, J., Jin, L., Yadav, A.K., Bansal, S., Mi, T., Hilakivi-Clarke, L., Clarke, R., Youngblood, B., Cheema, A., Verma, V., 2025. Pyruvate kinase M2 activation reprograms mitochondria in CD8 T cells, enhancing effector functions and efficacy of anti-PD1 therapy. Cell Metab. 37 (6), 1294–1310. https://doi.org/10.1016/j.cmet.2025.03.003. .e1297.

Moskophidis, D., Lechner, F., Pircher, H., Zinkernagel, R.M., 1993. Virus persistence in acutely infected immunocompetent mice by exhaustion of antiviral cytotoxic effector T cells. Nature 362 (6422), 758–761. https://doi.org/10.1038/362758a0.

Multhoff, G., Radons, J., Vaupel, P., 2014. Critical role of aberrant angiogenesis in the development of tumor hypoxia and associated radioresistance. Cancers 6 (2), 813–828. https://doi.org/10.3390/cancers6020813.

Peralta, R.M., Xie, B., Lontos, K., Nieves-Rosado, H., Spahr, K., Joshi, S., Ford, B.R., Quann, K., Frisch, A.T., Dean, V., Philbin, M., Cillo, A.R., Gingras, S., Poholek, A.C., Kane, L.P., Rivadeneira, D.B., Delgoffe, G.M., 2024. Dysfunction of exhausted T cells is enforced by MCT11-mediated lactate metabolism. Nat. Immunol. 25 (12), 2297–2307. https://doi.org/10.1038/s41590-024-01999-3.

Rougerie, P., Largeteau, Q., Megrelis, L., Carrette, F., Lejeune, T., Toffali, L., Rossi, B., Zeghouf, M., Cherfils, J., Constantin, G., Laudanna, C., Bismuth, G., Mangeney, M., Delon, J., 2013. Fam65b is a new transcriptional target of FOXO1 that regulates RhoA signaling for T lymphocyte migration. J. Immunol. 190 (2), 748–755. https://doi.org/10.4049/jimmunol.1201174.

Scharping, N.E., Rivadeneira, D.B., Menk, A.V., Vignali, P.D.A., Ford, B.R., Rittenhouse, N.L., Peralta, R., Wang, Y., Wang, Y., DePeaux, K., Poholek, A.C.,

Delgoffe, G.M., 2021. Mitochondrial stress induced by continuous stimulation under hypoxia rapidly drives T cell exhaustion. Nat. Immunol. 22 (2), 205–215. https://doi.org/10.1038/s41590-020-00834-9.

Shang, S., Yang, H., Fan, D., Deng, J., 2025. Combination of ginsenoside compound K and anti-PD1 inhibits pancreatic cancer by activating CXCL13-CXCR5 signaling axis. J. Agric. Food Chem. 73 (24), 15125–15137. https://doi.org/10.1021/acs.jafc.5c01821.

Sharma, P., Hu-Lieskovan, S., Wargo, J.A., Ribas, A., 2017. Primary, adaptive, and acquired resistance to cancer immunotherapy. Cell 168 (4), 707–723. https://doi.org/10.1016/j.cell.2017.01.017.

Singh, S., Barik, D., Arukha, A.P., Prasad, S., Mohapatra, I., Singh, A., Singh, G., 2023. Small molecule targeting immune cells: a novel approach for cancer treatment. Biomedicines. 11 (10). https://doi.org/10.3390/biomedicines11102621.

Wang, J., Li, R.-Z., Wang, W.-J., Pan, H.-D., Xie, C., Yau, L.-F., Wang, X.-X., Long, W.-L., Chen, R.-H., Liang, T.-L., Ma, L.-R., Li, J.-X., Huang, J.-M., Wu, Q.-B., Liu, L., He, J.-X., Leung, E.L.-H., 2023. CERS4 predicts positive anti-PD-1 response and promotes immunomodulation through Rhob-mediated suppression of CD8+Tim3+ exhausted T cells in non-small cell lung cancer. Pharmacol. Res. 194. https://doi.org/10.1016/j.phrs.2023.106850.

Wang, Y., Zeng, Y., Yang, W., Wang, X., Jiang, J., 2024. Targeting CD8+ T cells with natural products for tumor therapy: revealing insights into the mechanisms. Phytomedicine 129. https://doi.org/10.1016/j.phymed.2024.155608.

Won, H.-J., Kim, H.I., Park, T., Kim, H., Jo, K., Jeon, H., Ha, S.J., Hyun, J.M., Jeong, A., Kim, J.S., Park, Y.J., Eo, Y.H., Lee, J., 2019. Non-clinical pharmacokinetic behavior of ginsenosides. J. Ginseng. Res. 43 (3), 354–360. https://doi.org/10.1016/j.jgr.2018.06.001.

Wu, H., Zhao, X., Hochrein, S.M., Eckstein, M., Gubert, G.F., Knöpper, K., Mansilla, A.M., Öner, A., Doucet-Ladevèze, R., Schmitz, W., Ghesquière, B., Theurich, S., Dudek, J., Gasteiger, G., Zernecke, A., Kobold, S., Kastenmüller, W., Vaeth, M., 2023a. Mitochondrial dysfunction promotes the transition of precursor to terminally exhausted T cells through HIF-1α-mediated glycolytic reprogramming. Nat. Commun. 14 (1). https://doi.org/10.1038/s41467-023-42634-3.

Wu, J.E., Manne, S., Ngiow, S.F., Baxter, A.E., Huang, H., Freilich, E., Clark, M.L., Lee, J. H., Chen, Z., Khan, O., Staupe, R.P., Huang, Y.J., Shi, J., Giles, J.R., Wherry, E.J., 2023b. *In vitro* modeling of CD8 T cell exhaustion enables CRISPR screening to reveal a role for BHLHE40. Sci. Immunol. 8 (86). https://doi.org/10.1126/sciimmunol.ade3369.

Xu, Z., Wang, X., Cheng, H., Li, J., Zhang, X., Wang, X., 2025. The role of MCT1 in tumor progression and targeted therapy: a comprehensive review. Front. Immunol. 16. https://doi.org/10.3389/fimmu.2025.1610466.

Zehn, D., Thimme, R., Lugli, E., de Almeida, G.P., Oxenius, A., 2022. Stem-like' precursors are the fount to sustain persistent CD8+ T cell responses. Nat. Immunol. 23 (6), 836–847. https://doi.org/10.1038/s41590-022-01219-w.

Zhou, W., Qu, M., Yue, Y., Zhong, Z., Nan, K., Sun, X., Wu, Q., Zhang, J., Chen, W., Miao, C., 2024. Acetylcysteine synergizes PD-1 blockers against colorectal cancer progression by promoting TCF1+PD1+CD8+ T cell differentiation. Cell Commun. Signal. 22 (1). https://doi.org/10.1186/s12964-024-01848-8.